Composite Structures 96 (2013) 332–345

Contents lists available at SciVerse ScienceDirect

Composite Structures

journal homepage: www.elsevier.com/locate/compstruct

Robust C^k/C^0 generalized FEM approximations for higher-order conformity requirements: Application to Reddy's HSDT model for anisotropic laminated plates

Paulo de Tarso R. Mendonça *, Clovis S. de Barcellos, Diego Amadeu F. Torres

Group of Mechanical Analysis and Design – GRANTE, Department of Mechanical Engineering, Federal University of Santa Catarina, 88040-900 Florianópolis, SC, Brazil

ARTICLE INFO

Article history:
Available online 17 September 2012

Keywords:
Combined C^k/C^0 continuous approximations
GFEM
HSDT plate bending model
Enhanced transverse shear stresses

ABSTRACT

The Third-order Plate Theory proposed by Reddy for modeling laminated composite plates has earned wide acceptance in the engineering community. It involves the same five generalized displacement components $(u^o, v^o, w^o, \psi_x, \psi_y)$ as the first-order models (e.g. Mindlin's) and, at the same time, its higher-order expansion across the thickness enables it to provide more accurate displacements and layer-wise stress estimates. However, its FEM implementation is somewhat hindered by the need to employ a $C^1(\Omega)$ continuous basis for the transverse displacement w^o.

In this paper, an instance of the Generalized Finite Element Method, GFEM, which allows an arbitrary C^k continuity, is used to solve arbitrary anisotropic laminated composite plate bending problems.

The resultant basis functions naturally exhibit inter-element continuity and can be easily enriched to generate arbitrary p-enriched basis functions. These characteristics result in excellent abilities in terms of approximating the layer stresses. In particular, the high degree of the basis, combined with its continuity, enables the transverse shear stresses to be integrated from the local equilibrium equations, and also post-processed in a scaling operation explored by the authors to provide additional accuracy of the estimates across the thickness. Additionally, all of the estimated strain and stress fields are naturally continuous, without the need for any heuristic averaging or smoothing operation. The procedure is robust enough to allow for Partition of Unity (PoU) construction free of geometrical restrictions on the elements and it is suitable for mixed C^k/C^0 formulations, using continuous functions only for those variables which require such continuity, in order to reduce the computational cost.

The method is implemented with three-node triangular elements, and its performance is illustrated through comparisons with analytic solutions, with special emphasis on the computation of the transverse stress field for thick laminates.

1. Introduction

In recent decades, multilayered composite plates and shells have been increasingly applied in engineering design due to the well-known benefits they provide, particularly within the fields of aeronautics and smart/intelligent materials and structures [1–3]. In order to take advantage of its high specific strength and modulus, it must be possible to predict the behavior of these laminates. A first approach to investigating the integrity of this type of multiscale media would be to use a three-dimensional model in order to precisely capture the significant stresses which arise at the interfaces of the layered composites. However, this approach is limited because it requires enormous computing effort, besides computational difficulties when some layers are much thinner than others.

Hence, some simplified models have been used to solve practical problems applying finite and boundary element methods, as well as some analytic solutions in very simple cases. The simplest one is the Classical Laminate Theory, CLT, which is based on Kirchhoff's hypothesis in which the normal to the reference surface remains straight, undeformed and normal [4]. The next simplest is the First-order Shear Deformation Theory, FSDT, whose displacement field follows Mindlin's hypothesis [5] in which the normals remain straight and undeformed but not necessarily normal to the reference surface. These two-dimensional models are usually adequate for thin laminates. In order to improve the displacement description several higher-degree models have been proposed and, of these, Reddy's model [6] has become a very popular two-dimensional model due to its simplicity. All of the higher-order models consider the displacement components as nonlinear functions of the normal coordinate. Further improvements can be obtained with layer-wise theories, by assuming displacement fields with C^0 continuity along the normal coordinate between each pair of layers, and these theories are widely accepted for thick laminates, see, for instance [7–9].

* Corresponding author. Tel.: +55 48 3721 9899.
E-mail addresses: mendonca@grante.ufsc.br (Paulo de Tarso R. Mendonça), clovis@grante.ufsc.br (C.S. de Barcellos), diego.amadeu@gmail.com (Diego Amadeu F. Torres).

0263-8223/$ - see front matter © 2012 Elsevier Ltd. All rights reserved.
http://dx.doi.org/10.1016/j.compstruct.2012.09.004

In this paper, the Third-order Plate Theory proposed by Reddy [6] is used to model a laminated plate problem. This theory is similar to the CLT and FSDT, but with more elaborate assumptions concerning the in-plane displacements, which are described by cubic functions of the thickness coordinate. As shown in Section 2, transverse displacement is required to present C^1-continuity, as in the Kirchhoff's model. When using the conventional finite element method, FEM, this continuity requires intricate shape functions, see, for instance [10], with several degrees of freedom including nodal displacements, nodal rotations, and higher-order derivatives in order to obtain a compatible formulation. For this reason, other approaches have gained greater attention, such as the simpler (and C^0) Mindlin model, the non-conforming C^1 elements and hybrid and mixed variational formulations. The lack of simple and robust finite elements with C^1-continuity has led to the widespread development and use of several C^0-continuity elements, e.g. [11], and several mesh-free approaches like [12,13,10,14–16].

The most common schemes are those based on incompatible functions and Hermite functions are not adequate for *p*-refinement of the models. One alternative which provides a consistent formulation with arbitrary continuity was proposed by Duarte et al. [17] and involves constructing shape functions with arbitrary continuity through the use of the Edwards' scheme [18] and *R*-functions [19] as an instance of the Generalized Finite Element Method, GFEM. The GFEM, in turn, was independently proposed by Babuška and Melenk as an instance of the Partition of Unity (PoU) method, e.g. [20,21], and by Oden et al. [22] as a scheme for reducing the computing time of meshless methods like *hp*-Cloud. The meshless procedures usually use circles or spheres, as clouds, around each node with arbitrary radius, and each integration point is then covered by an arbitrary number of clouds. This obviously increases the cost of building the PoU. The main idea proposed in [22] is to substitute the circular clouds with an arbitrarily-shaped polygonal cloud defined as the union of elements connected to the associated node "α". As a result, the PoU is known beforehand since it is a global FEM shape function and the enrichments are performed in exactly the same way as in the *hp*-Cloud Method. The same procedure, from the mathematical point of view, was later denoted by XFEM, see, for instance, Belytschko et al. [23] and Moës et al. [24], with emphasis on applications with discontinuity fields.

In this paper, an instance of the Generalized Finite Element Method, GFEM, based on Duarte's scheme [17], is used to generate arbitrary, C^k-continuous basis functions which are used to solve an arbitrary anisotropic laminated composite plate, based on Reddy's kinematic model, as a test of its suitability for interlaminar shear stress estimation. This C^k-GFEM implementation is based on Shepard's PoU with at least C^k continuity and is enrichments according to the *hp*-Cloud Method. The weighting functions used in Shepard's PoU are built as products of C^∞ edge functions of the distance of such a point to each of the cloud boundaries through the Edwards procedure [18] for convex clouds. For non-convex clouds, a boolean composition of these edge functions, following Rvachev [25], may be adopted as proposed by Duarte [17].

The basis functions thus generated are continuous at inter-element interfaces and can be easily enriched to generate arbitrary *p*-enriched basis. These characteristics result in an excellent capacity to approximate the layer stresses. In particular, the high degrees obtained with *p*-enrichment allow for better solutions for the stress across the thickness, despite using single-layer plate models as demonstrated by Torres et al. [26]. The high continuity of the basis, in turn, enables that the transverse shear stresses can be integrated from the local equilibrium equations, and also be post-processed, in a scaling operation proposed by the authors, to provide additional accuracy of the estimates across the thickness. Additionally, all of the estimated strain and stress fields are naturally continuous, without the need for any heuristic averaging or smoothing procedure. An example is used to illustrate the ability of the formulation to approximate the stress field continuously.

The remainder of this paper is outlined as follows: Section 2 summarizes Reddy's kinematic plate model; Section 3 briefly presents the construction of PoU functions with the desired continuity and the enrichment procedure used to enhance the ansatz space; and Section 4 presents the results for the proposed formulation in order to test its behavior under some combinations of continuity and enrichment. Finally, Section 5 summarizes some conclusions.

2. Reddy's kinematic plate model

This plate bending model was proposed by Reddy [6] and is one of the higher order shear deformation plate theories, HSDT, intended to improve the description of the complex displacement field across the thickness of laminated plates as compared to the CLT and FSDT. As a matter of completeness, the main aspects of this model are summarized in the present section.

Let us consider a laminate occupying a region V defined in a three-dimensional Cartesian coordinate system $\mathcal{R}^3$, with a plane middle surface, Ω, bounded by a closed Lipschitzian contour, Γ, and with a constant thickness $H > 0$. Hence, the domain can be described by

$$V = \left\{ (\boldsymbol{x}, z) \in \mathcal{R}^3 | z \in \left[\frac{-H}{2}, \frac{H}{2}\right], \boldsymbol{x} \in \Omega \right\}, \tag{1}$$

where $\boldsymbol{x} = (x, y)$ and $\Omega \subset \mathcal{R}^2$. Reddy's Third-order Plate Theory is characterized by the following displacement assumption

$$\begin{aligned} u(x,y,z) &= u^0(x,y) + z\psi_x(x,y) - c_1 z^3 \left(\psi_x(x,y) + \frac{\partial w^0(x,y)}{\partial x}\right) \\ v(x,y,z) &= v^0(x,y) + z\psi_y(x,y) - c_1 z^3 \left(\psi_y(x,y) + \frac{\partial w^0(x,y)}{\partial y}\right) \\ w(x,y,z) &= w^0(x,y), \end{aligned} \tag{2}$$

where u, v, and w are the displacement components along the x, y, and z directions, respectively, $u^0(x,y)$ and $v^0(x,y)$ are inplane displacements of the middle surface, $w^0(x,y)$ is the transverse displacement, and $\psi_x(x,y)$ and $\psi_y(x,y)$ are the rotations undergone by a straight segment initially normal to the reference surface, about the x and y axes, respectively, in a similar fashion to that in FSDT. Here, the normal does not remain normal after the deformation as in lower-order models, but if one defines c_1 as equal to zero, one recovers the Mindlin model. In Reddy's model c_1 is set to equal $4/(3H^2)$, which ensures zero transverse shear strains on both faces ($z = \pm H/2$) of the laminate.

Substituting this displacement field into the linear strain–displacement relations results in the non-vanishing deformation components being the in-plane deformations $\boldsymbol{\epsilon}(x,y,z) = \{\epsilon_x, \epsilon_y, \gamma_{xy}\}^T$ (the superscript T indicates transpose) and the transverse shear deformations $\boldsymbol{\gamma}_c(x,y,z) = \{\gamma_{yz}, \gamma_{xz}\}^T$. According to Eq. (2), the in-plane deformations are related to displacements by

$$\boldsymbol{\epsilon}(x,y,z) = \boldsymbol{\epsilon}^0(x,y) + z\boldsymbol{\kappa}^1(x,y) + z^3\boldsymbol{\kappa}^3(x,y), \tag{3}$$

where $\boldsymbol{\epsilon}^0(x.y)$ and $\boldsymbol{\kappa}^1(x,y)$ are the membrane deformations and changes in curvatures of the reference surface, respectively, and $\boldsymbol{\kappa}^2(x,y)$ is the higher-order curvature. The transverse shear deformations are given by

$$\boldsymbol{\gamma}_c(x,y,z) = \boldsymbol{\gamma}^0(x,y) + z^2\boldsymbol{\gamma}^2(x,y), \tag{4}$$

where $\boldsymbol{\gamma}^0(x,y)$ are the shear strains and $\boldsymbol{\gamma}^2(x,y)$ are the shear-warping strains.

Denoting the generalized displacement vector $\boldsymbol{u} = \{u^0, v^0, w^0, \psi_x, \psi_y\}^T$, one can write $\boldsymbol{\epsilon}^0 = \boldsymbol{L}^0 \cdot \boldsymbol{u}$, $\boldsymbol{\kappa}^1 = \boldsymbol{L}^1 \cdot \boldsymbol{u}$, $\boldsymbol{\kappa}^3 = \boldsymbol{L}^3 \cdot \boldsymbol{u}$, $\boldsymbol{\gamma}^0 = \boldsymbol{L}^{s0} \cdot \boldsymbol{u}$, $\boldsymbol{\gamma}^2 = \boldsymbol{L}^{s2} \cdot \boldsymbol{u}$, where $\boldsymbol{L}^0$, $\boldsymbol{L}^1$, $\boldsymbol{L}^3$, $\boldsymbol{L}^{s0}$, and $\boldsymbol{L}^{s2}$ are differential operators given by

$$\boldsymbol{L}^0=\begin{bmatrix}\frac{\partial}{\partial x}&0&0&0&0\\0&\frac{\partial}{\partial y}&0&0&0\\\frac{\partial}{\partial y}&\frac{\partial}{\partial x}&0&0&0\end{bmatrix},\quad \boldsymbol{L}^1=\begin{bmatrix}0&0&0&\frac{\partial}{\partial x}&0\\0&0&0&0&\frac{\partial}{\partial y}\\0&0&0&\frac{\partial}{\partial y}&\frac{\partial}{\partial x}\end{bmatrix},$$
$$\boldsymbol{L}^3=\begin{bmatrix}0&0&-c_1\frac{\partial^2}{\partial x^2}&-c_1\frac{\partial}{\partial x}&0\\0&0&-c_1\frac{\partial^2}{\partial y^2}&0&-c_1\frac{\partial}{\partial y}\\0&0&-2c_1\frac{\partial^2}{\partial x\partial y}&\frac{\partial}{\partial y}&\frac{\partial}{\partial x}\end{bmatrix},\quad \boldsymbol{L}^{s0}=\begin{bmatrix}0&0&\frac{\partial}{\partial y}&0&1\\0&0&\frac{\partial}{\partial x}&1&0\end{bmatrix},$$
$$\boldsymbol{L}^{s2}=\begin{bmatrix}0&0&-3c_1\frac{\partial}{\partial y}&0&-3c_1\\0&0&-3c_1\frac{\partial}{\partial x}&-3c_1&0\end{bmatrix}. \tag{5}$$

The in-plane and transverse shear stress components are denoted by $\boldsymbol{\sigma}=\{\sigma_x,\sigma_y,\sigma_{xy}\}^T$ and $\boldsymbol{\tau}_s=\{\tau_{yz},\tau_{xz}\}^T$, respectively. The Generalized Hooke's Law for an arbitrary layer k, in the plane stress state, can be written as

$$\boldsymbol{\sigma}=\overline{\boldsymbol{Q}}\epsilon, \tag{6}$$

where $\overline{\boldsymbol{Q}}$ is a 3×3 reduced stiffness matrix representing the orthotropic layer with its principal material directions arbitrarily oriented with respect to axis x [4]. Similarly, the transverse shear stress–strain relation for an arbitrary layer k can be described as $\boldsymbol{\tau}_s=\boldsymbol{C}_s\boldsymbol{\gamma}_s$, where $\boldsymbol{C}_s$ is the 2×2 reduced transverse shear stiffness matrix of a layer. The resultant inplane forces $\boldsymbol{N}=\{N_x,N_y,N_{xy}\}^T$, resultant moments $\boldsymbol{M}=\{M_x,M_y,M_{xy}\}^T$, resultant transverse forces $\boldsymbol{Q}=\{Q_y,Q_x\}^T$, and resultant higher-order stresses $\boldsymbol{P}=\{P_x,P_y,P_{xy}\}^T$ and $\boldsymbol{R}=\{R_y,R_x\}^T$ are defined as

$$\boldsymbol{N}=\int_{z=-H/2}^{H/2}\boldsymbol{\sigma}\,dz,\quad \boldsymbol{M}=\int_{z=-H/2}^{H/2}z\boldsymbol{\sigma}\,dz,$$
$$\boldsymbol{P}=\int_{z=-H/2}^{H/2}z^3\boldsymbol{\sigma}\,dz,\quad \boldsymbol{Q}=\int_{z=-H/2}^{H/2}\boldsymbol{\tau}_s\,dz,\quad \boldsymbol{R}=\int_{z=-H/2}^{H/2}z^2\boldsymbol{\tau}_s\,dz. \tag{7}$$

By using the reduced Hooke's Law, these definitions lead to the relation between resultant forces and moments with mid-surface deformations of the laminate

$$\begin{Bmatrix}\boldsymbol{N}\\\boldsymbol{M}\\\boldsymbol{P}\end{Bmatrix}=\begin{bmatrix}\boldsymbol{A}&\boldsymbol{B}&\boldsymbol{E}\\\boldsymbol{B}&\boldsymbol{D}&\boldsymbol{F}\\\boldsymbol{E}&\boldsymbol{F}&\boldsymbol{H}\end{bmatrix}\begin{Bmatrix}\boldsymbol{\epsilon}^0\\\boldsymbol{\kappa}^1\\\boldsymbol{\kappa}^3\end{Bmatrix}, \tag{8}$$

where $\boldsymbol{A},\boldsymbol{B},\boldsymbol{D},\boldsymbol{E},\boldsymbol{F}$ and $\boldsymbol{H}$ are 3×3 stiffness sub-matrices, all symmetric, representing in-plane, bending and stretch-bending coupling behavior of the laminated plate. The transverse resultant forces are given by

$$\begin{Bmatrix}\boldsymbol{Q}\\\boldsymbol{R}\end{Bmatrix}=\begin{bmatrix}\boldsymbol{A}_s&\boldsymbol{D}_s\\\boldsymbol{D}_s&\boldsymbol{F}_s\end{bmatrix}\begin{Bmatrix}\boldsymbol{\gamma}^0\\\boldsymbol{\gamma}^2\end{Bmatrix}, \tag{9}$$

where $\boldsymbol{A}_s$, $\boldsymbol{D}_s$ and $\boldsymbol{F}_s$ are 2×2 stiffness sub-matrices representing the transverse shear behavior of the laminate. These matrix components are obtained by integration across the thickness in the following way

$$\{A_{ij},B_{ij},D_{ij},E_{ij},F_{ij},H_{ij}\}=\sum_{k=1}^{N}\int_{z_{k-1}}^{z_k}\overline{Q}_{ij}^k\{1,z,z^2,z^3,z^4,z^6\}dz,\quad i,\ j=1,\ 2,\ 3. \tag{10}$$

$$\{A_{s_{ij}},D_{s_{ij}},F_{s_{ij}}\}=\sum_{k=1}^{N}\int_{z_{k-1}}^{z_k}C_{s_{ij}}^k\{1,z^2,z^4\}dz,\quad i,\ j=1,\ 2. \tag{11}$$

In cases where the laminate is symmetric with respect to the reference surface, the coupling stiffness matrices $\boldsymbol{B}$ and $\boldsymbol{E}$ are both null and, therefore, the bending response is decoupled from the in-plane behavior. For a complete reference, see [4].

The formulation implemented in this paper is aimed at the general case of laminated plates composed of anisotropic layers, represented by Eqs. (2)–(9), through a generalized finite element procedure. Therefore, let us start from the bilinear and linear operators

$$\mathcal{B}(\boldsymbol{u},\hat{\boldsymbol{u}})=\int_\Omega\begin{Bmatrix}\hat{\boldsymbol{\epsilon}}^0\\\hat{\boldsymbol{\kappa}}^1\\\hat{\boldsymbol{\kappa}}^3\end{Bmatrix}^T\begin{bmatrix}\boldsymbol{A}&\boldsymbol{B}&\boldsymbol{E}\\\boldsymbol{B}&\boldsymbol{D}&\boldsymbol{F}\\\boldsymbol{E}&\boldsymbol{F}&\boldsymbol{H}\end{bmatrix}\begin{Bmatrix}\boldsymbol{\epsilon}^0\\\boldsymbol{\kappa}^1\\\boldsymbol{\kappa}^3\end{Bmatrix}d\Omega + \int_\Omega\begin{Bmatrix}\hat{\boldsymbol{\gamma}}^0\\\hat{\boldsymbol{\gamma}}^2\end{Bmatrix}^T\begin{bmatrix}\boldsymbol{A}_s&\boldsymbol{D}_s\\\boldsymbol{D}_s&\boldsymbol{F}_s\end{bmatrix}\begin{Bmatrix}\boldsymbol{\gamma}^0\\\boldsymbol{\gamma}^2\end{Bmatrix}d\Omega,\ \mathcal{L}(\hat{w})=\int_\Omega\hat{w}^0q_z\,d\Omega, \tag{12}$$

where q_z is the z-component of distributed force. Hence, the plate problem can be stated in a weak form as: *find* $\boldsymbol{u}(x,y)\in\mathcal{U}_1(\Omega)$, *such that*

$$\mathcal{B}(\boldsymbol{u},\hat{\boldsymbol{u}})=\mathcal{L}(\hat{w}^0),\quad \text{for }\forall\hat{\boldsymbol{u}}\in\mathcal{V}_1 \tag{13}$$

where $\mathcal{U}_1\subset\mathcal{H}^0(\Omega)\times\mathcal{H}^0(\Omega)\times\mathcal{H}^1(\Omega)\times\mathcal{H}^0(\Omega)\times\mathcal{H}^0(\Omega)$ is the set of kinematically admissible functions, $\mathcal{V}_1\subset\mathcal{H}^1(\Omega)$ is the space of admissible variation fields $\hat{\boldsymbol{u}}$, and $\mathcal{H}^m$ is the Hilbert space of order m, in which lie all of the functions that, together with their derivatives up to m order, are Lebesgue square integrable. The kinematic boundary conditions are $\boldsymbol{u}=\bar{\boldsymbol{u}}$, where $\bar{\boldsymbol{u}}$ is used to denote prescribed displacement and rotation values.

As in FEM, the discretization is performed element-wise by approximating the displacement field $\boldsymbol{u}(x,y)$ by $\boldsymbol{u}=\overline{\boldsymbol{N}}(\boldsymbol{x},\boldsymbol{y})\boldsymbol{d}^e$, where $\boldsymbol{d}^e$ is the vector containing the element degrees of freedom and $\overline{\boldsymbol{N}}(x,y)$ is the matrix of approximation functions. The deformations of the middle surface are discretized from Eqs. (3)–(5), which results in

$$\begin{Bmatrix}\boldsymbol{\epsilon}^0\\\boldsymbol{\kappa}^1\\\boldsymbol{\kappa}^3\end{Bmatrix}=\begin{bmatrix}\boldsymbol{B}^0\\\boldsymbol{B}^1\\\boldsymbol{B}^3\end{bmatrix}\boldsymbol{d}^e\quad\text{and}\quad\begin{Bmatrix}\boldsymbol{\gamma}^0\\\boldsymbol{\gamma}^2\end{Bmatrix}=\begin{bmatrix}\boldsymbol{B}^{s0}\\\boldsymbol{B}^{s2}\end{bmatrix}\boldsymbol{d}^e, \tag{14}$$

where $\boldsymbol{B}^0$, $\boldsymbol{B}^1$, $\boldsymbol{B}^3$, $\boldsymbol{B}^{s0}$, and $\boldsymbol{B}^{s2}$ are generalized strain matrices, respectively, given by

$$\begin{cases}\boldsymbol{B}^0=\boldsymbol{L}^0\overline{\boldsymbol{N}}\\\boldsymbol{B}^1=\boldsymbol{L}^1\overline{\boldsymbol{N}}\\\boldsymbol{B}^3=\boldsymbol{L}^3\overline{\boldsymbol{N}}\end{cases}\quad\text{and}\quad\begin{matrix}\boldsymbol{B}^{s0}=\boldsymbol{L}^{s0}\overline{\boldsymbol{N}},\\\boldsymbol{B}^{s2}=\boldsymbol{L}^{s1}\overline{\boldsymbol{N}}.\end{matrix} \tag{15}$$

The element stiffness matrix is evaluated in the standard way by

$$\boldsymbol{K}^e=\int_{\Omega^e}\left\{\begin{bmatrix}\boldsymbol{B}^0\\\boldsymbol{B}^1\\\boldsymbol{B}^3\end{bmatrix}^T\begin{bmatrix}\boldsymbol{A}&\boldsymbol{B}&\boldsymbol{E}\\\boldsymbol{B}&\boldsymbol{D}&\boldsymbol{F}\\\boldsymbol{E}&\boldsymbol{F}&\boldsymbol{H}\end{bmatrix}\begin{bmatrix}\boldsymbol{B}^0\\\boldsymbol{B}^1\\\boldsymbol{B}^3\end{bmatrix}+\begin{bmatrix}\boldsymbol{B}^{s0}\\\boldsymbol{B}^{s2}\end{bmatrix}^T\begin{bmatrix}\boldsymbol{A}_s&\boldsymbol{D}_s\\\boldsymbol{D}_s&\boldsymbol{F}_s\end{bmatrix}\begin{bmatrix}\boldsymbol{B}^{s0}\\\boldsymbol{B}^{s2}\end{bmatrix}\right\}d\Omega. \tag{16}$$

After superposing the element stiffness matrices and consistent element load vectors, the equilibrium equations for static problems reduce to the standard form $\boldsymbol{K}\boldsymbol{d}=\boldsymbol{f}$, where $\boldsymbol{K}$ is the global stiffness matrix, $\boldsymbol{d}$ is the global degrees-of-freedom vector and $\boldsymbol{f}$ is the equivalent nodal load vector added by concentrated external loads. After solving for $\boldsymbol{d}$, one can compute the displacements, strain, and stresses and the resultant forces and moments. Low-order elements may present shear locking, such that usually some scheme must be introduced in order to circumvent it. However, in this paper, none such scheme was utilized, and both terms in the element stiffness matrix, membrane-bending, and transverse shear stiffness parts, are equally integrated with the same quadrature.

The evaluation of the in-plane stresses is performed directly from the constitutive equations. However, it is well known that the transverse shear stresses obtained from the constitutive equations are too poor to be useful. The most popular procedure to extract these stresses is by integrating the two local differential

equilibrium equations for forces in the x and y directions, in the absence of body forces:

$$\begin{aligned}\frac{\partial\sigma_x}{\partial x}+\frac{\partial\tau_{xy}}{\partial y}+\frac{\partial\tau_{xz}}{\partial z}=0,\\ \frac{\partial\tau_{xy}}{\partial x}+\frac{\partial\sigma_y}{\partial y}+\frac{\partial\tau_{yz}}{\partial z}=0.\end{aligned} \tag{17}$$

Expressions for the x and y differentiation of $\boldsymbol{B}^0$, $\boldsymbol{B}^1$, and $\boldsymbol{B}^3$ are easily obtained, such that the first equation in (14) can be differentiated and derivatives of $\boldsymbol{\epsilon}^0$, $\boldsymbol{\kappa}^1$, and $\boldsymbol{\kappa}^3$ can be obtained. Next, derivatives of the inplane stresses in an arbitrary position z within each layer k are computed from

$$\begin{aligned}\frac{\partial\boldsymbol{\sigma}}{\partial x}=\overline{\boldsymbol{Q}}^k\left\{\frac{\partial\boldsymbol{\epsilon}^0}{\partial x}+z\frac{\partial\boldsymbol{\kappa}^1}{\partial x}+z^3\frac{\partial\boldsymbol{\kappa}^3}{\partial x}\right\},\\ \frac{\partial\boldsymbol{\sigma}}{\partial y}=\overline{\boldsymbol{Q}}^k\left\{\frac{\partial\boldsymbol{\epsilon}^0}{\partial y}+z\frac{\partial\boldsymbol{\kappa}^1}{\partial y}+z^3\frac{\partial\boldsymbol{\kappa}^3}{\partial y}\right\}.\end{aligned} \tag{18}$$

The transverse shear stresses estimates are obtained by integrating each one of the equations in (17), using the derivatives of the inplane stresses in (18), and applying the boundary conditions $\tau_{xz}(x,y,z=-H/2)=\tau_{yz}(x,y,z=-H/2)=0$. Therefore, the transverse shear stresses in a coordinate z within a layer k, are given by

$$\begin{aligned}\tau^k_{xz}(\boldsymbol{x},z)=\tau^k_{xz}(\boldsymbol{x},z_{k-1})-\int_{z=z_{k-1}}^{z}(\sigma_{x,x}+\tau_{xy,y})dz,\\ \tau^k_{yz}(\boldsymbol{x},z)=\tau^k_{yz}(\boldsymbol{x},z_{k-1})-\int_{z=z_{k-1}}^{z}(\tau_{xy,x}+\sigma_{y,y})dz,\end{aligned} \tag{19}$$

for $z_{k-1}\leqslant z\leqslant z_k$, where $\boldsymbol{x}=(x,y)$, z_{k-1} and z_k are the z coordinates of the lower and upper surfaces of the layer k and, as is usually the case, the layer numbering begins at the "lower" surface of the laminate ($z_0=-H/2$) and ends at the top ($z_N=H/2$). The integration is performed layer by layer, starting from the first one, and the following continuity conditions are applied at the layer interfaces: $\tau^k_{xz}(x,y,z_{k-1})=\tau^{k-1}_{xz}(x,y,z_{k-1})$ and $\tau^k_{yz}(x,y,z_{k-1})=\tau^{k-1}_{yz}(x,y,z_{k-1})$.

2.1. Scaling of the integrated shear stresses

The heuristic process of obtaining improved transverse shear stresses by integration of the local equilibrium equations has been complemented by the authors [27] with a second step, aiming to gain a higher level of accuracy of the estimate. The procedure requires that, at a given surface point (x,y), the shear forces Q_x and Q_y are computed from the constitutive equations, and also that the shear forces Q^i_x and Q^i_y are computed from the integration of the integrated transverse shear stresses τ^k_{xz} and τ^k_{yz} obtained from (19). Thus, both sets of shear forces are used to compute correction factors at the point (x,y)

$$R_x=\frac{Q_x}{Q^i_x}\ \text{and}\ R_y=\frac{Q_y}{Q^i_y}. \tag{20}$$

The last step of the procedure consists of applying the correction factors to scale the entire distribution of integrated shear stresses at (x,y) as

$$\tau^c_{xz}=R_x\tau^k_{xz}\ \text{and}\ \tau^c_{yz}=R_y\tau^k_{yz}, \tag{21}$$

with τ^c_{xz} and τ^c_{yz} being the scaled transverse shear stresses.

This construction is based on the assumption that the variation in the stresses across the thickness have a "good" level of quality, which is inherited from the local character of the local equilibrium equations. However, the processing of these stresses requires the first derivatives of the in-plane stresses, which reduces the resulting accuracy of the shear stresses thus computed. However, the shear forces computed directly from the constitutive equations do not require any further differentiation of the stresses, which means that they basically have the same level of accuracy as the in-plane stresses, which is a direct consequence of the degree of the approximation functions. The scaling performed in (21) aims to introduce part of this accuracy of the constitutive shear forces into the integrated shear stresses. The results obtained so far seem to verify that this is indeed the case.

The procedure to compute the integrated shear forces is summarized as follows. Firstly, it should be noted that the explicit integration in z in (19) is obtained from the integration of (18)

$$\begin{aligned}\int_{z_{k-1}}^{z}\frac{\partial\boldsymbol{\sigma}}{\partial x}dz=\overline{\boldsymbol{Q}}^k\Big\{(z-z_{k-1})\frac{\partial\boldsymbol{\epsilon}^0}{\partial x}+\frac{1}{2}(z^2-z^2_{k-1})\frac{\partial\boldsymbol{\kappa}^1}{\partial x}\\ +\frac{1}{4}(z^4-z^4_{k-1})\frac{\partial\boldsymbol{\kappa}^3}{\partial x}\Big\},\\ \int_{z_{k-1}}^{z}\frac{\partial\boldsymbol{\sigma}}{\partial y}dz=\overline{\boldsymbol{Q}}^k\Big\{(z-z_{k-1})\frac{\partial\boldsymbol{\epsilon}^0}{\partial y}+\frac{1}{2}(z^2-z^2_{k-1})\frac{\partial\boldsymbol{\kappa}^1}{\partial y}\\ +\frac{1}{4}(z^4-z^4_{k-1})\frac{\partial\boldsymbol{\kappa}^3}{\partial y}\Big\}.\end{aligned} \tag{22}$$

This suggests that the integrated shear stresses have a polynomial variation of quartic degree across the layer thickness for Reddy's model, whereas it is easy to observe that this variation is quadratic in Mindlin's model. The shear force is obtained from a second integration over the thickness of each layer, from $z_0=-H/2$ to $z_N=H/2$

$$\begin{aligned}Q^i_x(z_k)=Q^i_x(z_{k-1})+h_k\tau^k_{xz}(z_{k-1})-\int_{\check{z}=z_{k-1}}^{z_k}\left[\int_{z=z_{k-1}}^{\check{z}}(\sigma_{x,x}+\tau_{xy,y})dz\right]d\check{z},\\ Q^i_y(z_k)=Q^i_y(z_{k-1})+h_k\tau^k_{yz}(z_{k-1})-\int_{\check{z}=z_{k-1}}^{z_k}\left[\int_{z=z_{k-1}}^{\check{z}}(\tau_{xy,x}+\sigma_{y,y})dz\right]d\check{z},\end{aligned} \tag{23}$$

where $Q^i_x(z_0)=Q^i_y(z_0)=0$, h_k is the thickness of layer k and z_{k-1} and z_k are the z coordinates of the lower and upper surface of layer k. The terms under the integrands on the right-hand side can be obtained from

$$\begin{aligned}\int_{\check{z}=z_{k-1}}^{z_k}\int_{z=z_{k-1}}^{\check{z}}\frac{\partial\boldsymbol{\sigma}}{\partial x}dz\,d\check{z}=\overline{\boldsymbol{Q}}^k\left\{a_k\frac{\partial\boldsymbol{\epsilon}^0}{\partial x}+b_k\frac{\partial\boldsymbol{\kappa}^1}{\partial x}+c_k\frac{\partial\boldsymbol{\kappa}^3}{\partial x}\right\},\\ \int_{\check{z}=z_{k-1}}^{z_k}\int_{z=z_{k-1}}^{\check{z}}\frac{\partial\boldsymbol{\sigma}}{\partial y}dz\,d\check{z}=\overline{\boldsymbol{Q}}^k\left\{a_k\frac{\partial\boldsymbol{\epsilon}^0}{\partial y}+b_k\frac{\partial\boldsymbol{\kappa}^1}{\partial y}+c_k\frac{\partial\boldsymbol{\kappa}^3}{\partial y}\right\},\end{aligned} \tag{24}$$

where

$$\begin{aligned}a_k&=\frac{1}{2}(z^2_k-z^2_{k-1})-z_{k-1}h_k,\\ b_k&=\frac{1}{2}\left[\frac{1}{3}(z^3_k-z^3_{k-1})-z^2_{k-1}h_k\right],\\ c_k&=\frac{1}{4}\left[\frac{1}{5}(z^5_k-z^5_{k-1})-z^4_{k-1}h_k\right].\end{aligned} \tag{25}$$

From (19) it can be noted that, in order to obtain accurate transverse shear stresses, it is essential to have not only accurate in-plane stresses but also accurate estimates of their derivatives along the x and y axes. It is also clear from (5) that the in-plane displacements and the rotations fields require at least C^0 continuity and the transverse displacement, w^0, C^1 continuity in FEM approximations. If one is interested in evaluating the transverse shear stresses along interelement boundaries, continuous stress fields need to be used in (19). In this case, the displacement fields are required to have an additional order of continuity which is not available in conventional FEM and GFEM, which is one of the motivations behind this study. The next section describes the generation of arbitrarily continuous approximation functions.

3. GFEM C^k approximation functions

In this instance of the Generalized Finite Element Method, GFEM, the aim is to use approximation functions with arbitrary continuity, k, not only to meet the C^1-continuity in arbitrary domain triangulations, as required by conforming elements under Reddy's assumption, but also to be able to describe continuous stress fields. This is very useful in evaluating transverse shear stresses by integrating local equilibrium equations everywhere. Toward this goal and using the *hp*-Cloud strategy of enrichment, approximation functions which approach zero need to be built, together with their k first normal derivatives, as the cloud boundary is approached. This procedure is similar to that for Kirchhoff's model presented in [28].

In order to summarize this procedure, let us consider a conventional finite element triangulation, $\{\mathcal{K}_e\}_{e=1}^{NE}$ (NE being the number of elements in $\mathcal{K}_e$), defined by Nnodes with coordinates $\{\boldsymbol{x}_\alpha\}_{\alpha=1}^{N}$, in an open-bounded domain $\Omega \subset \mathcal{R}^2(\boldsymbol{x})$. For each of these nodes, one denotes the interior of the union of the finite elements sharing it as a *cloud*, $\omega_\alpha,\ \alpha = 1,\ \ldots,\ N$, as usually denoted in GFEM. Over each cloud, C^k appropriate weighting functions are evaluated and used in the Shepard's Moving Least Square Method [29] scheme for generating a Partition of Unity, as describe in the following.

3.1. Partition of unity

Let an open-bounded domain $\Omega \subset \mathcal{R}^2(\boldsymbol{x})$, here defined as the plate mid-surface, and let $\Im_N$ be an open covering of this domain built by the set of N clouds ω_α, associated with the nodes $\boldsymbol{x}_\alpha$, that is, the closure $\overline{\Omega}$ of the domain is contained in the union of the cloud closures $\overline{\omega}_\alpha$:

$$\overline{\Omega} \subset \cup_{\alpha=1}^{N} \overline{\omega}_\alpha. \tag{26}$$

In addition, consider next a set of functions $\mathcal{S}_N = \{\varphi_\alpha(\boldsymbol{x})\}_{\alpha=1}^{N}$, each having the corresponding cloud ω_α as its compact support. If this set has the property that each one of these functions is such that $\varphi_\alpha(\boldsymbol{x}) \in C_0^k(\omega_\alpha),\ k \geqslant 0$ and $\sum_{i=1}^{N} \varphi_\alpha(\boldsymbol{x}) = 1,\ \forall \boldsymbol{x} \in \Omega$, and every compact subset of Ω intersects only a finite number of supports, then the set $\{\varphi_\alpha(\boldsymbol{x})\},\ \alpha = 1,\ \ldots,\ N$ is said to be a Partition of Unity, PoU, subordinated to the covering $\Im_N$ [30]. The first requirement indicates that a function φ_α is non-zero only over its respective cloud ω_α and is, at least, k times continuously differentiable.

There are several kinds of PoU used in computational mechanics and the FEM shape functions are just one type, which is in $C_0^0(\omega_\alpha)$. Additional examples can be found in several meshless methods, such as the *hp*-Cloud method. Another example, the Shepard scheme, makes use of *weighting functions*, $\mathcal{W}_\alpha : \mathcal{R}^2 \to \mathcal{R}$, with the cloud ω_α as their compact support, such that $\mathcal{W}_\alpha$ belongs to the space $C_0^k(\omega_\alpha)$. The Shepard PoU functions subordinated to the covering $\Im_N$ are defined as

$$\varphi_\alpha(\boldsymbol{x}) = \frac{\mathcal{W}_\alpha(\boldsymbol{x})}{\sum_{\beta(\boldsymbol{x})} \mathcal{W}_\beta(\boldsymbol{x})},\quad \beta(\boldsymbol{x}) \in \{\gamma | \mathcal{W}_\gamma(\boldsymbol{x}) \neq 0\}. \tag{27}$$

Therefore, the regularity of these PoU functions relies only on the regularity of the weighting functions and, when using the Reddy plate model, functions belonging to at least $C^1(\Omega)$ are required. In several meshless methods circular (in 2-D) or spherical (in 3-D) neighborhoods are used as clouds, where one-dimensional functions of the distance to the cloud node are used as weighting functions. These functions are quite simple and decay to zero as the distance from the node increases. This procedure has the disadvantage of high computational cost, since one has to determine which clouds cover each integration point. Aiming to reduce the computational time, the GFEM scheme uses element meshes to define the clouds, but this reduces the continuity of the weighting functions, defined as follows (see also [17], in the case of non-convex clouds).

Once the edge functions $\varepsilon_{\alpha j}(\xi_j)$ are defined (see details in [28]), the weighting function for a convex cloud ω_α is then defined as the product of all cloud edge functions as defined by

$$\mathcal{W}_\alpha(\boldsymbol{x}) := \prod_{j=1}^{M_\alpha} \varepsilon_{\alpha j}(\xi_j), \tag{28}$$

where M_α is the number of cloud edge functions associated with the cloud ω_α. For illustration, suppose a node αwhose polygonal cloud is built by the union of five triangular elements as shown in Fig. 1 and is bounded by five edges. To define the edge functions, let us consider an arbitrary point $P$with coordinates $\boldsymbol{x}$ whose distance to an edge j is given by

$$\xi_j(\boldsymbol{x}) = \boldsymbol{n}_{\alpha j} \cdot (\boldsymbol{x} - \boldsymbol{b}_{\alpha j}), \tag{29}$$

where $\boldsymbol{n}_{\alpha j}$ is the edge normal vector pointing toward the cloud interior and $\boldsymbol{b}_{\alpha j}$ is a point at the boundary j, e.g. its midpoint. Thus, the *cloud edge function* is a function which vanishes, together with its k derivatives, as this edge is approached and is strictly positive in the interior of the cloud. Many functions meet these requirements and in [28] polynomials and exponential functions were subjected to numerical investigations. Herein, exponential edge functions are used, which guarantee $C^\infty(\Omega)$ on convex clouds.

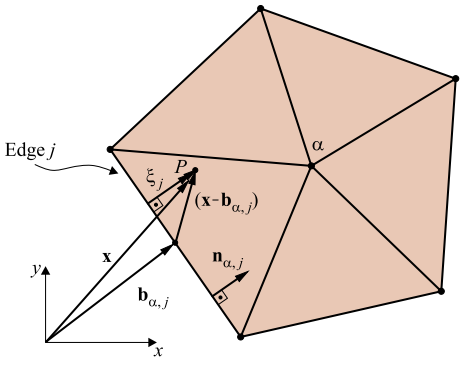

Fig. 1. Node α and its cloud formed by five elements. Normal coordinate ξ_j of a point P associated with edge j.

3.2. Enrichment and approximation functions

The PoU functions can be enriched by multiplying anyone of them by a set of enrichment functions, $\{L_{i\alpha}\}_{i\in\mathcal{I}(\alpha)}$, where $\mathcal{I}(\alpha),\ \alpha = 1,\ \ldots,\ N$, is an index set of known functions, for instance, polynomials, generalized harmonic functions, boundary layer functions, particular solutions to similar problems, singular solutions to the specific problem under consideration, and anisotropic functions. Thus, the local approximation subspaces can be denoted as $\chi_\alpha(\omega_\alpha) = span\{L_{i\alpha}\}_{i\in\mathcal{I}(\alpha)}$ which may also be enriched according to an adaptive method.

In this study, due to the simple types of loading and geometry, uniform polynomial enrichments are chosen such that

$$\mathcal{P}_p(\omega_\alpha) \subset \chi_\alpha^p(\omega_\alpha),$$

where $\mathcal{P}_p$ stands for the space of polynomials of degree less than or equal to p. The numerical experiments indicated that to improve the condition number of the global stiffness matrix, a scaling of the basis at the cloud level can be carried out. Herein, this scaling is performed considering a characteristic length h_α of the cloud, which can be taken as the largest distance from the node $\boldsymbol{x}_\alpha$ to each of the cloud ω_α edges, or some approximation of it. Thus, one can define the intrinsic coordinate $\bar{\boldsymbol{x}}$ as $\bar{\boldsymbol{x}} = (\boldsymbol{x} - \boldsymbol{x}_\alpha)/h_\alpha$, the origin of which is at node $\boldsymbol{x}_\alpha$ and which attains a maximum value of unity at some

cloud edge. Therefore, considering an arbitrary node $\boldsymbol{x}_\alpha$, the approximation functions defined in its cloud are $\phi_i^\alpha = \varphi_\alpha(\boldsymbol{x})L_{i\alpha}(\bar{\boldsymbol{x}})$, where the enrichment sets considered in the results shown in this paper are the following:

$$\begin{aligned}\text{Enrichment : Cubic} \quad & L_{i\alpha} = [1,\bar{x},\bar{y},\bar{x}^2,\bar{x}\bar{y},\bar{y}^2,\bar{x}^3,\bar{x}^2\bar{y},\bar{x}\bar{y}^2,\bar{y}^3],\\ \text{Quartic} \quad & L_{i\alpha} = [1,\bar{x},\bar{y},\bar{x}^2,\bar{x}\bar{y},\bar{y}^2,\bar{x}^3,\bar{x}^2\bar{y},\bar{x}\bar{y}^2,\bar{y}^3,\bar{x}^4,\\ & \bar{x}^3\bar{y},\bar{x}^2\bar{y}^2,\bar{x}\bar{y}^3,\bar{y}^4].\end{aligned} \tag{30}$$

Thus, denoting by $\mathcal{U}_h \subset \mathcal{U}_1$ the subspace spanned by a set of kinematically admissible GFEM approximation functions and $\mathcal{V}_h$ the respective subspace of admissible variations, the Galerkin approximation is given by: *find* $\boldsymbol{u}(\boldsymbol{x}) \in \mathcal{U}_h(\Omega)$, *such that* $\mathcal{B}(\boldsymbol{u},\hat{\boldsymbol{u}}) = \mathcal{L}(\hat{\boldsymbol{u}})$, *for* $\forall \hat{\boldsymbol{u}} \in \mathcal{V}_1$, where $\boldsymbol{u}$ and $\hat{\boldsymbol{u}}$ are described by

$$\boldsymbol{u}(\boldsymbol{x}) = \sum_{\alpha=1}^{N}\varphi_\alpha(\boldsymbol{x})\left\{d_\alpha + \sum_{i=1}^{q_j}L_{i\alpha}(\bar{\boldsymbol{x}})b_{i\alpha}\right\} = \boldsymbol{\Phi}D \tag{31}$$

$$\hat{\boldsymbol{u}}(\boldsymbol{x}) = \sum_{\alpha=1}^{N}\varphi_\alpha(\boldsymbol{x})\left\{v_\alpha + \sum_{i=1}^{q_j}L_{i\alpha}(\bar{\boldsymbol{x}})c_{i\alpha}\right\} = \boldsymbol{\Phi}\widetilde{V} \tag{32}$$

d_α and v_α are nodal values, and $b_{i\alpha}$ and $c_{i\alpha}$ are generalized nodal coefficients associated with the enrichment functions. $\boldsymbol{D}$ and $\boldsymbol{V}$ are 1-D arrays of nodal values and coefficients obtained from $d_\alpha, v_\alpha, b_{i\alpha}$ and $c_{i\alpha}$ values, and $\boldsymbol{\Phi}(x,y)$ is an array formed by the basis functions.

Remark 1. When the PoU is built from polynomial finite element shape functions, as in conventional GFEM, the system of equations resulting from Eqs. (31) and (32) is linearly dependent [31]. In the present case, where the PoU is built as quotients of exponential functions, the resulting global stiffness matrix is positive definite if the boundary conditions imposed are sufficient to prevent rigid body motions.

Remark 2. It should be observed that the usual structure of the standard displacement-based FEM is preserved in the present formulation, represented by the discrete form of the formulation summarized in Section 2. The entire GFEM C^k formulation, summarized in the present section, enters the program structure encapsulated in a single routine, which computes the set of approximate functions as in the case of the FEM functions, which is to be used normally in the computation of the $\boldsymbol{B}$ matrices and the element stiffness matrix.

4. Numerical results

The evaluation of the scheme is performed considering the standard problem of a square simply-supported laminate under sinusoidal load, which possesses an analytic solution for Reddy's kinematic model. The geometric characteristics of the plate are (Fig. 2): sides a, total thickness H such that $a/H = 4$, which means an extremely case of thick plate. There are three equal layers oriented as [0°/90°/0°], with properties E_1 = 175 GPa, E_2 = 7 GPa, $G_{12} = G_{13}$ = 3.5 GPa, G_{23} = 1.4 GPa and $\nu_{12} = \nu_{13} = \nu_{23} =$ 0.25. The distributed transverse load is given by $q_z(x,y) = q\sin(\pi x/a)\sin(\pi y/a)$. It shoud be noted that the formulation described herein is adequate for arbitrary anisotropic laminates, and the choice of a simply-supported square symmetric example is due only to the availability of a complete analytic solution for the same kinematic model. Four meshes were used, defined by a mesh index M, the meaning of which is provided in Fig. 2.

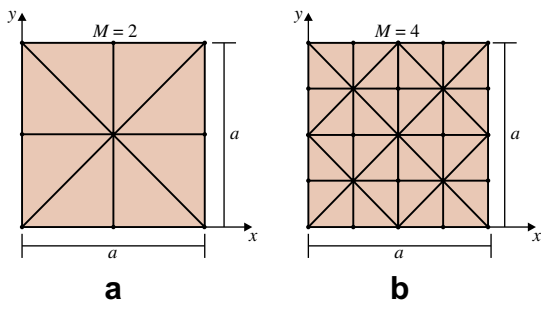

Fig. 2. Illustration of the meshes associated with mesh indices $M = 2$ and $M = 4$.

As shown in Mendonça et al. [27], the continuous PoU is only capable of reproducing a unitary constant function over the domain, while the discontinuous PoU of the standard GFEM is able to generate a complete polynomial of one degree over the domain. Therefore, when the GFEM C^k PoU is enriched with a polynomial set of degree j, the approximation functions form a basis for polynomials of degree $b = j$. On the other hand, when a discontinuous GFEM C^0 PoU is enriched with a polynomial set of degree j, the approximation functions form a basis for polynomials of degree $b = j + 1$.

The results reported in this paper were obtained with enrichment functions of degrees $p = 3$ and 4, due to the emphasis on the computation of transverse shear stresses, which requires second derivatives of the displacements. Since only the transverse displacement w^0 requires at least C^1 functions, whereas the normal rotations ψ_x and ψ_y can be modeled with C^0 functions, two possibilities arise and were tested:

1. Formulation described as GFEM C^k/C^k $p = (j,j)$ (or simply GFEM C^k $p = j$), where both transverse displacement and rotations are modeled with C^∞ PoU and enriched with polynomials up to degree j.
2. Formulation described as GFEM C^k/C^0 $p = (j,j-1)$, where the transverse displacement is modeled with C^∞ PoU and the rotations with standard C^0 PoU with enrichment polynomials up to j and $j-1$ degrees, respectively. In this case, in order to reduce the computational cost, the use of C^∞ PoU only for the variable that requires such continuity and C^0 PoU for the other variables is recommended. The standard C^0 PoU is based on piecewise continuous functions that are tent-like PoU inside each cloud, such as standard FEM shape functions.

Therefore, in relation to the second formulation above, it should be noted that when the rotations are enriched with polynomials of degree $p = j - 1$, the resulting functions span the space of polynomial functions of degree $b = j$, which is the same degree as that of the continuous basis used for w^0. Consequently, it is possible to have less degrees of freedom while keeping the basis degree b. The discontinuous GFEM basis functions are faster to compute than the continuous ones, leading to an interest in testing their behavior when associated with their continuous counterpart.

4.1. Performance assessment through strain energy: influence of integration and discretization

The continuous basis functions generated by the procedure described in Section 3 are highly oscillatory, requiring a large amount of integration points for the stiffness matrix computation. Fig. 3 investigates the integrability of the stiffness matrix, computing a normalized strain energy, as E/E_{ref}, versus the number of integration points NIP, where $E$is the strain energy, defined as $\frac{1}{2}\int_V \boldsymbol{\varepsilon} : \boldsymbol{\sigma}\, dV$, and NIP is the square root of the total number of integration points used in each element. The mesh used is that with index $M = 6$ (according to Fig. 2). The results are normalized with respect to a reference va-

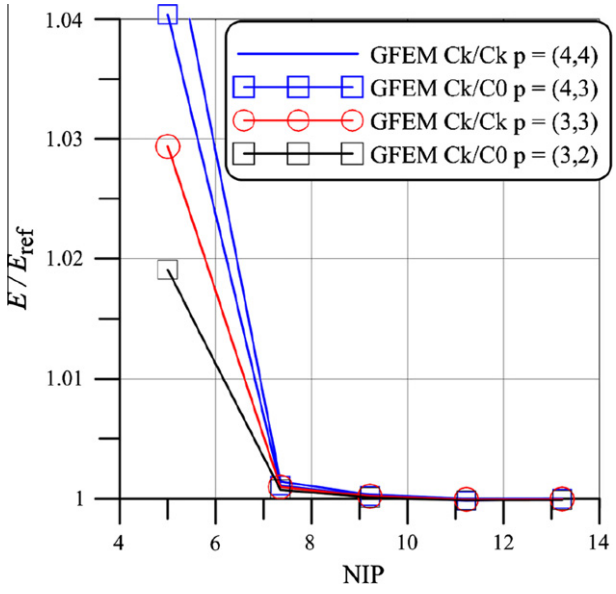

Fig. 3. Normalized strain energy E/E_{ref} versus number of integration points NIP. Values normalized to E_{ref} obtained with NIP = 13.2. Triangle integration rule. Edge function: exponential. $a/H = 4$. Mesh index $M = 6$.

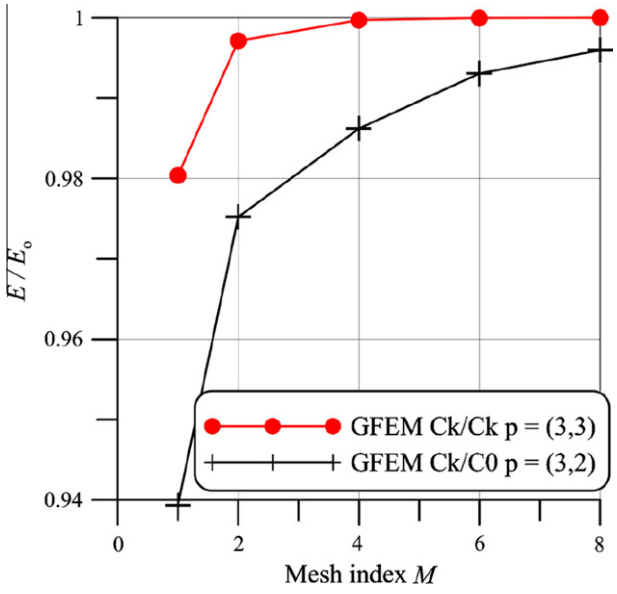

Fig. 4. Normalized strain energy E/E_0 versus mesh index M, for enrichment degrees $p = 2$ and 3, and degree of the basis $b = 3$. Triangle integration rule with NIP = 13.2. Edge function exponential. $a/H = 4$.

lue E_{ref}, computed with NIP = 13.2. All results shown in this text were obtained with Wandzura's triangle integration rule [32]. Fig. 3 shows the accuracy of the results with NIP for C^k/C^k $p = (4,4)$ and C^k/C^0 $p = (4,3)$, which are associated with basis functions of degree $b = 4$, and C^k/C^k $p = (3,3)$ and C^k/C^0 $p = (3,2)$, which are associated with basis functions of degree $b = 3$. The numerical data in Table 1 show that, as expected, the higher degrees are more penalized by sub integration. In general, the observations are similar to those associated with the Kirchhoff problem [28], which also requires C^1 functions. It should be noted that NIP $\simeq 9$ is generally sufficient in a routinely analysis with $b = 3$.

Figs. 4 and 5 show the evolution of such normalized strain energy with the mesh index M and the degree b of the basis, for both continuous GFEM C^k and mixed GFEM C^k/C^0. In this case, E_0 is the analytic value of the strain energy. For integration purposes the largest amount of integration points was used, that is NIP = 13.2. From both figures it can be seen that, even though the basis for both C^k/C^k $p = (3,3)$ and C^k/C^0 $p = (3,2)$ is degree $b = 3$, the presence of the discontinuous functions in the approximation of the rotations reduces the accuracy obtained, mainly for coarse meshes. The same effect is seen in Fig. 5 for $b = 4$, although less pronounced.

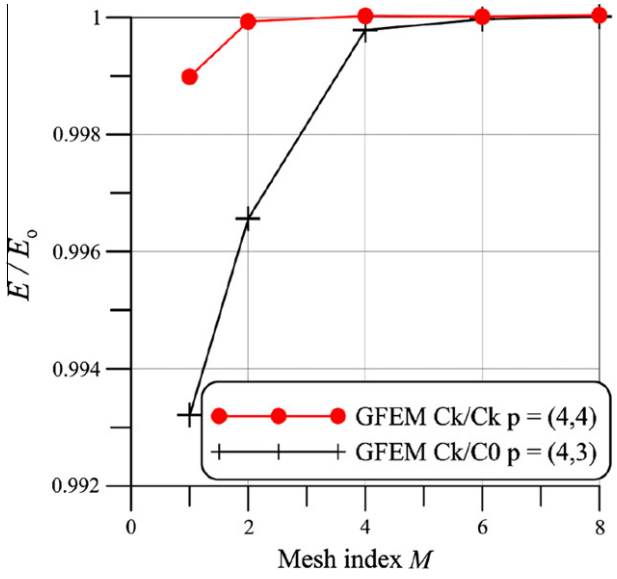

Fig. 5. Normalized strain energy E/E_0 versus mesh index M, for enrichment degrees $p = 3$ and 4, and degree of the basis $b = 4$. Triangle integration rule with NIP = 13.2. Edge function exponential. $a/H = 4$.

4.2. Performance evaluation on point-wise values

In the following, the viability of the proposed C^k/C^0 formulation is discussed through the evaluation of point-wise values of in-plane stresses as well as transverse shear stresses (constitutive, integrated and integrated/scaled) and shear forces.

Fig. 6 shows the variation of the normalized in-plane stress $\sigma_{xo} = \sigma_x H^2/(qa^2)$ across the thickness, at the center plate point $(x, y) = (a/2; a/2)$. The basis functions are of degree $b = 3$ for both continuous GFEM C^k and mixed GFEM C^k/C^0 formulations, and the results are excellent when compared with the analytical results. The results for enrichments $p = (4,4)$ and $p = (4,3)$, which generate basis functions of degree $b = 4$ for C^k and C^k/C^0 formulations, respectively, are not displayed to avoid superposition of curves.

Figs. 7 and 8 show the normalized transverse shear stresses $\tau_{xzo} = \tau_{xz} H/qa$ across the thickness, at a mid-side point $(x, y) = (a; a/2)$. The results, were obtained using only continuous

Table 1
Normalized strain energy E/E_{ref} versus number of integration points NIP. Values normalized to E_{ref} obtained with $NIP = 13.2$. Triangle integration rule. Edge function: exponential. $a/H = 4$.

NIP	C^k/C^k $p = (4,4)$	C^k/C^0 $p = (4,3)$	C^k/C^k $p = (3,3)$	C^k/C^0 $p = (3,2)$
5.	1.049271	1.040387	1.029366	1.019051
7.35	1.001432	1.001092	1.000972	1.000736
9.22	1.000322	1.000220	1.000199	0.999848
11.22	0.999982	0.999804	0.999920	0.999848
13.23	1.	0.999989	0.999942	0.999864

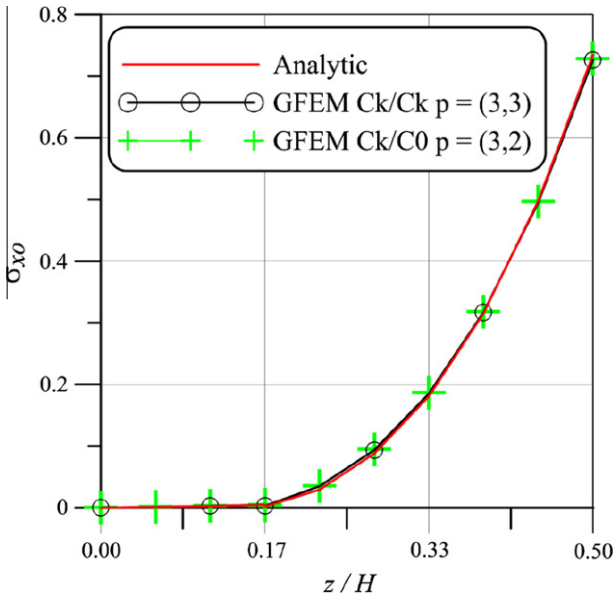

Fig. 6. Normalized in-plane stress $\sigma_{xo} = \sigma_x H^2/(qa^2)$ across the thickness, at point $(x,y) = (a/2; a/2)$. Triangle integration rule with NIP = 11.2. Mesh index $M = 6$. Edge function: exponential. $a/H = 4$.

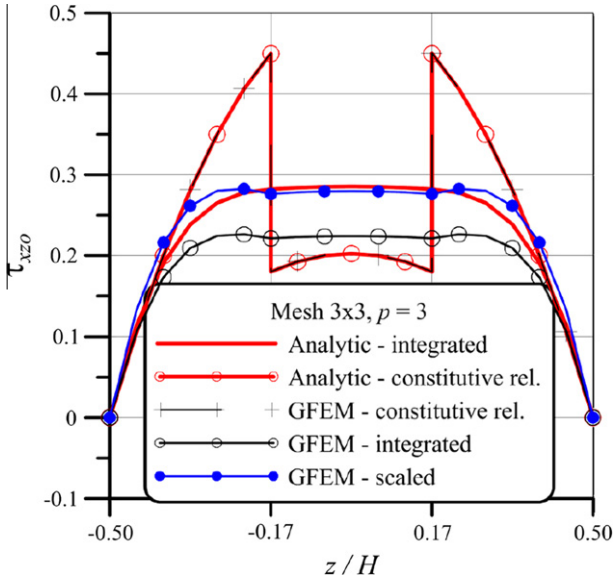

Fig. 7. Normalized transverse shear stresses $\tau_{xzo} = \tau_{xz} H/qa$ across the thickness, at point $(x,y) = (a; a/2)$, using only C^k basis. Triangle integration rule with NIP = 13.2. $M = 6$. Edge function: exponential. $a/H = 4,\ p = 3,\ b = 3$.

basis functions for w^0, ψ_x and ψ_y, with enrichment polynomials of degree $p = 3$ and 4 and, consequently, basis functions of degrees $b = 3$ and 4, respectively, and mesh index $M = 6$. Five types of results are shown for the transverse shear stresses:

1. Analytic solution obtained from the constitutive equations;
2. Analytic solution obtained integrating the analytic solutions of in-plane stresses, according to Eq. (19);
3. GFEM approximations obtained from constitutive equations;
4. GFEM approximations obtained from integration of the GFEM approximations of in-plane stresses, according to Eq. (19); and
5. GFEM approximations obtained post-processing the integrated results using the scaling procedure, as described in Section 2.1.

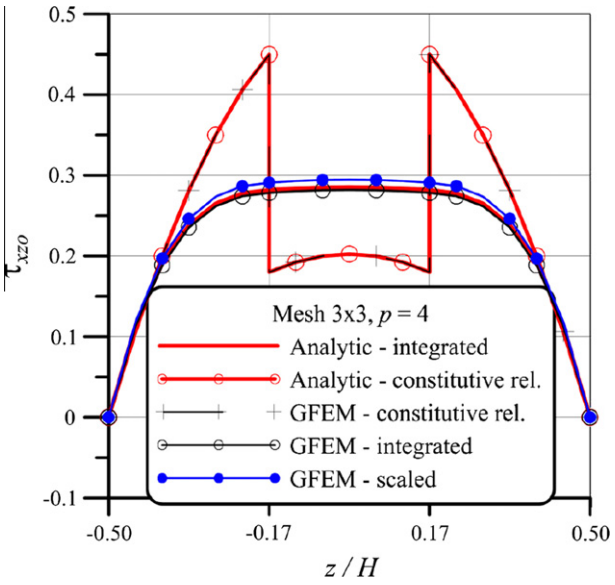

Fig. 8. Normalized transverse shear stresses $\tau_{xzo} = \tau_{xz} H/qa$ across the thickness, at point $(x,y) = (a; a/2)$, using only C^k basis. Triangle integration rule with NIP = 13.2. $M = 6$. Edge function: exponential. $a/H = 4,\ p = 4,\ b = 4$.

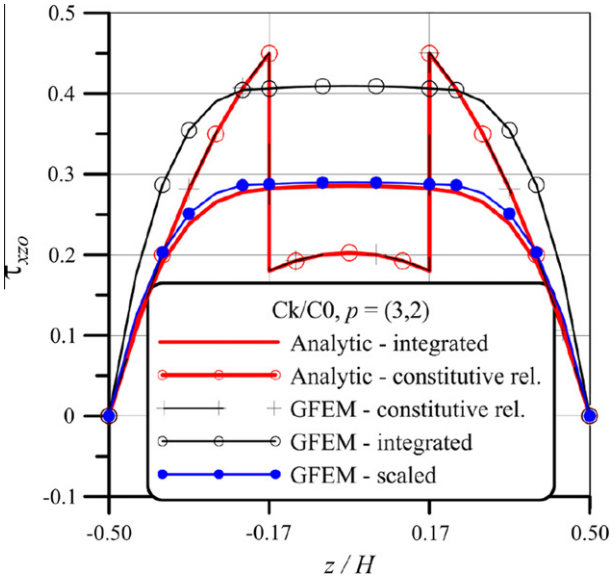

Fig. 9. Normalized transverse shear stresses $\tau_{xzo} = \tau_{xz} H/qa$ across the thickness, at point $(x,y) = (a; a/2)$, using C^k/C^0 formulation. Triangle integration rule with NIP = 13.2. $M = 6$. Edge function: exponential. $a/H = 4,\ p = (3,2),\ b = 3$.

Firstly, it can be noted that the GFEM approximations for the transverse shear stresses at the point are in excellent agreement with the analytic solutions obtained from constitutive equations. This is the same type of accuracy expected for the in-plane stresses. However, the constitutive analytic solution to the kinematic model itself is not physically realistic (it lacks interlayer continuity of the transverse shear stresses), and traditionally these stresses are obtained by integration of the local equilibrium equations. Since the integration procedure involves differentiation of the in-plane stresses, it requires the third derivatives of the transverse displacement w^0, as can be seen from Eqs. (2), (3), (6) and (19). Thus, the finite element formulations must be of high enough order such that their basis functions have meaningful third derivatives in or-

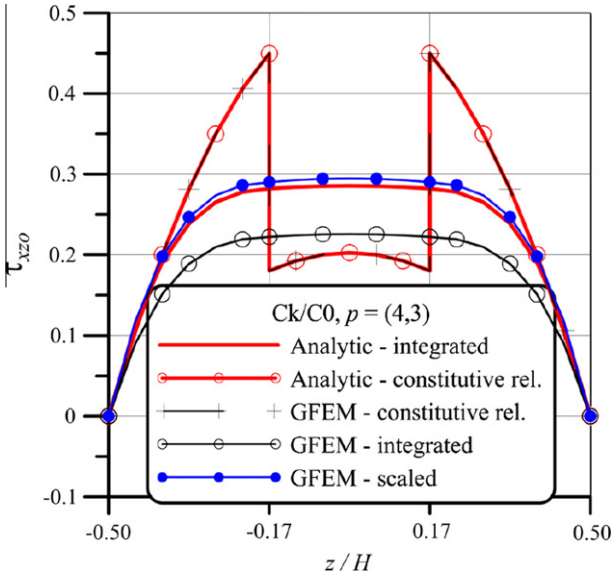

Fig. 10. Normalized transverse shear stresses $\tau_{xzo} = \tau_{xz}H/qa$ across the thickness, at point $(x,y) = (a;a/2)$, using C^k/C^0 formulation. Triangle integration rule with NIP = 13.2. $M = 6$. Edge function: exponential. $a/H = 4,\ p = (4,3),\ b = 4$.

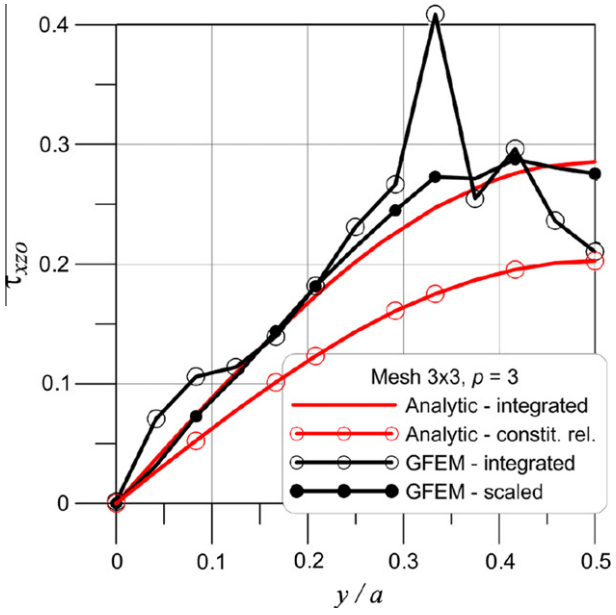

Fig. 11. Normalized transverse shear stresses $\tau_{xzo} = \tau_{xz}H/qa$ along the edge $(x,y) = (a;y)$, using only C^k basis. Triangle integration rule with NIP = 13.2. $M = 6$. Edge function: exponential. $a/H = 4,\ p = 3,\ b = 3$.

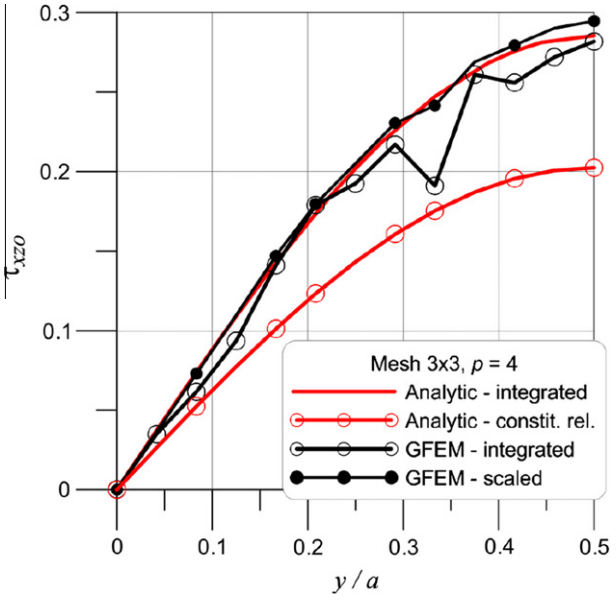

Fig. 12. Normalized transverse shear stresses $\tau_{xzo} = \tau_{xz}H/qa$ along the edge $(x,y) = (a;y)$, using only C^k basis. Triangle integration rule with NIP = 13.2. $M = 6$. Edge function: exponential. $a/H = 4,\ p = 4,\ b = 4$.

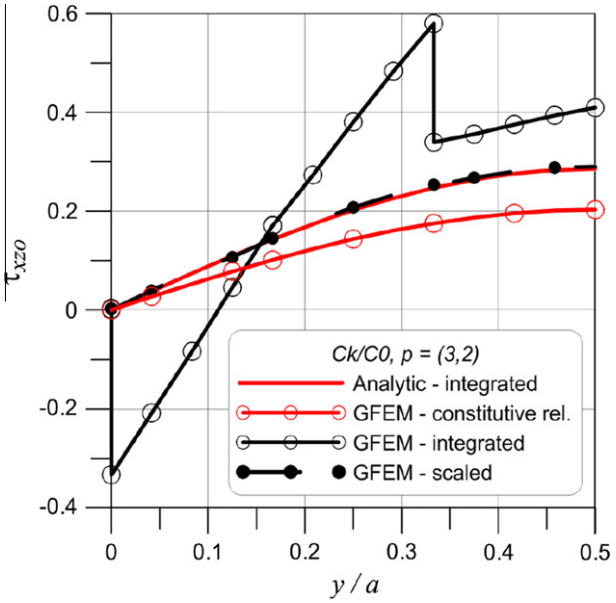

Fig. 13. Normalized transverse shear stresses $\tau_{xzo} = \tau_{xz}H/qa$ along the edge $(x,y) = (a;y)$, using C^k/C^0 basis. Triangle integration rule with NIP = 13.2. $M = 6$. Edge function: exponential. $a/H = 4,\ p = (3,2),\ b = 3$.

der to adequately estimate the transverse shear stresses. The results in Figs. 7 and 8 reveal that the GFEM C^k $p = 3$ provides acceptable estimates of the integrated transverse shear stress across the thickness. This is surprising, considering that the basis only spans polynomial spaces with a degree of at most $b = 3$, and the procedure involves three derivatives of the basis functions. As expected, the GFEM C^k $p = 4$ shows better results. This scenario effect was identified by Ramesh et al. [33], who used standard triangular elements of degree 8, with 45 nodes, to approximate the Mindlin bending plate model. In this case, the higher degree was shown to be essential to capture the effects of natural (force) boundary conditions on the transverse shear forces and twisting moments.

Even though the integration procedure (19) is well known and used, Fig. 7 shows that the scaling procedure can improve dramatically the quality of the approximation. An initial comparison between the scaled results in Figs. 7 and 8, for degrees $b = 3$ and 4, respectively, suggests that the scaling procedure was less efficient for $b = 3$ than for $b = 4$. However, these figures show only the response at a single point, at the mid-side position, at $(x,y) = (a;a/2)$.

In an attempt to further investigate the performance of the proposed C^k/C^0 formulation, the normalized transverse shear stresses $\tau_{xzo} = \tau_{xz}H/qa$ across the thickness, at a mid-side point $(x,y) = (a;a/2)$, using a continuous basis for w^0 and discontinuous

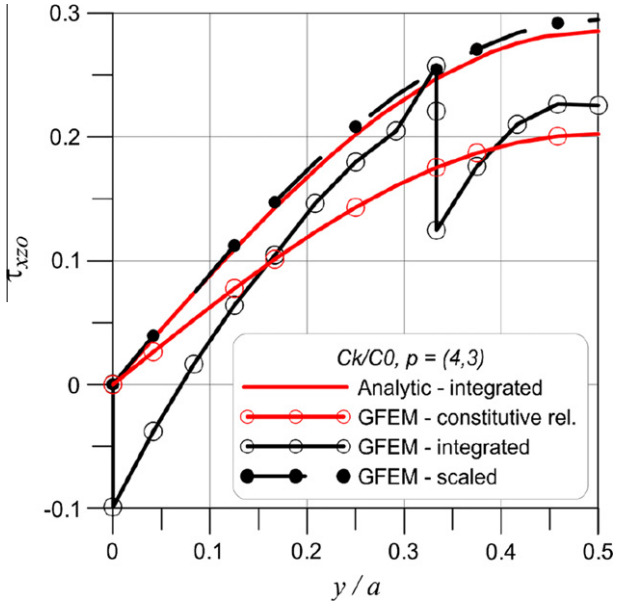

Fig. 14. Normalized transverse shear stresses $\tau_{xzo} = \tau_{xz}H/qa$ along the edge $(x,y) = (a;y)$, using C^k/C^0 basis. Triangle integration rule with NIP = 13.2. $M = 6$. Edge function: exponential. $a/H = 4,\ p = (4,3),\ b = 4$.

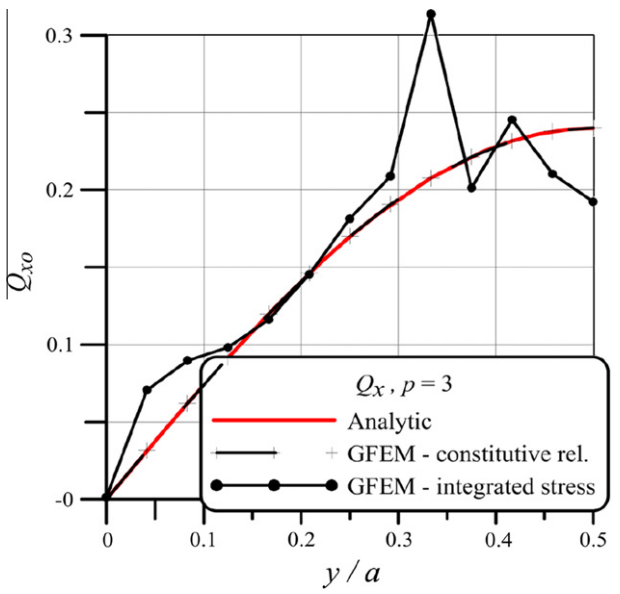

Fig. 15. Normalized shear force $Q_{xo} = Q_{xz}/qa$ along the edge $(x,y) = (a;y)$, using C^k basis. Triangle integration rule with NIP = 13.2. $M = 6$. Edge function: exponential. $a/H = 4,\ p = 3,\ b = 3$.

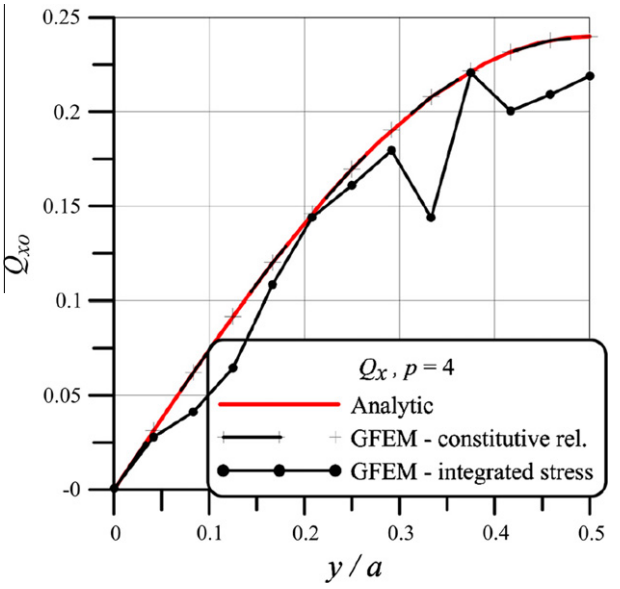

Fig. 16. Normalized shearforce $Q_{xo} = Q_{xz}/qa$ along the edge $(x,y) = (a;y)$, using C^k basis. Triangle integration rule with NIP = 13.2. $M = 6$. Edge function: exponential. $a/H = 4,\ p = 4,\ b = 4$.

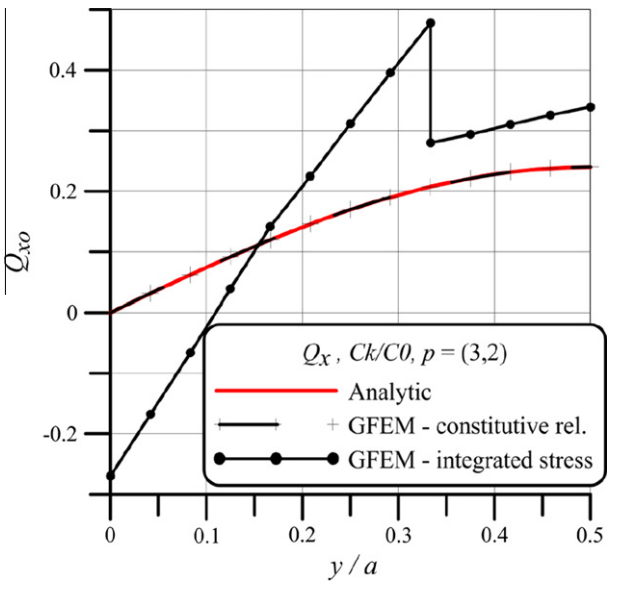

Fig. 17. Normalized shear force $Q_{xo} = Q_{xz}/qa$ along the edge $(x,y) = (a;y)$, using C^k/C^0 basis. Triangle integration rule with NIP = 13.2. $M = 6$. Edge function: exponential. $a/H = 4,\ p = (3,2),\ b = 3$.

ones for ψ_x and ψ_y, are displayed in Figs. 9 and 10. The results were obtained with enrichment polynomials of degree $p = 3$ and 4, respectively, in such a way that the resulting basis have degrees of $b = 3$ and 4. It should be noted that the integrated and scaled transverse shear stresses using the C^k/C^0 strategy are as good as those shown in Figs. 7 and 8, which verifies the applicability of the mixed C^k/C^0 procedure.

Figs. 11 and 12 show a more general view, where the normalized transverse shear stresses $\tau_{xzo} = \tau_{xz}H/qa$ along the edge $(x,y) = (a;y)$ and at the reference surface $z = 0$ are displayed. It can be seen that the cubic basis generates an oscillatory response to the integrated stresses, even when using only C^k functions, which is greatly improved by the scaling procedure. The quality of both approximations is better, as expected, with the basis of degree $b = 4$ seen in Fig. 12. Figs. 11–22 were produced from data computed on a uniform grid of five points along the side of each element. This results in sharp peaks in the integration results for $b = 3$, as seen in Fig. 11.

The normalized transverse shear stresses $\tau_{xzo} = \tau_{xz}H/qa$, along the edge $(x,y) = (a;y)$ and at the reference surface $z = 0$, when using the mixed C^k/C^0 formulation is shown in Figs. 13 and 14. It can be seen that the constitutive transverse shear stresses are continuous along the edge since their calculation involves in-plane derivatives only of w^0, which is modeled with the C^k basis (see (5)). Nevertheless, the integrated transverse shear stresses, which

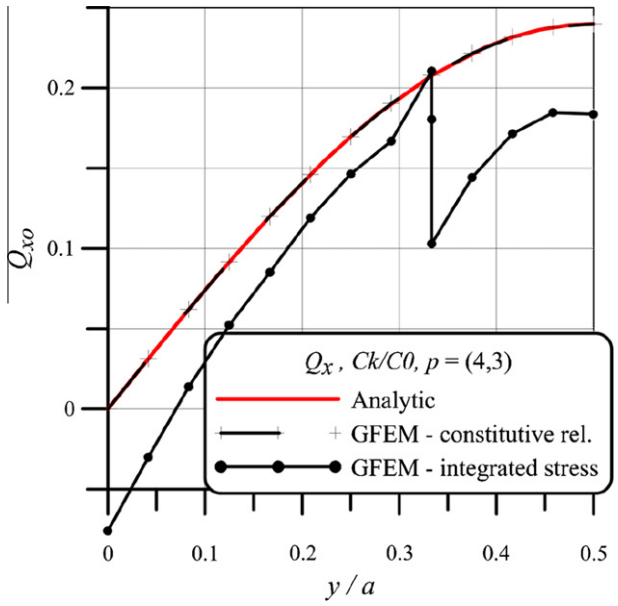

Fig. 18. Normalized shear force $Q_{xo} = Q_{xz}/qa$ along the edge $(x,y) = (a;y)$, using C^k/C^0 basis. Triangle integration rule with NIP = 13.2. $M = 6$. Edge function: exponential. $a/H = 4, p = (4,3), b = 4$.

require derivatives of in-plane stress components, are discontinuous as a consequence of the C^0 functions used for ψ_x and ψ_y, in contrast to Figs. 11 and 12. However, in the scaled values discontinuity is greatly reduced, and the overall results are in agreement with the analytic results.

The shear forces were then verified at the boundary and Figs. 15 and 16 show the results for the normalized shear forces $Q_{xo} = Q_x/qa$ along the edge $(x,y) = (a;y)$ when using only the C^k basis, for $p = b = 3$ and $p = b = 4$, respectively. It can be noted that the constitutive shear force obtained numerically matches very well the analytic solution, as a direct consequence of the guaranteed continuity for w^0 (see Eq. (5)) and the polynomial degree chosen for the basis. On the other hand, the shear forces obtained from the integration of the transverse shear stresses obtained from integration of the equilibrium Eq. (19), even though continuous, exhibit oscillations, due to the higher-order differentiations involved. Notably, the oscillations are less pronounced for $b = 4$ than for $b = 3$.

Figs. 17 and 18 show the normalized shear forces for the C^k/C^0 formulation using $p = (3,2)$ and $p = (4,3)$, respectively. In these cases, since ψ_x and ψ_y are modeled with the discontinuous basis, the shear forces obtained from integrated transverse shear stresses are discontinuous along the edge. The constitutive counterpart matches very well the analytic solution, as seen in Figs. 15 and 16.

It was noted that the scaling process corrects well the transverse shear stress distribution even in cases where the shear forces are discontinuous and oscillatory along the edges, which supports the motivation and hypothesis cited in Section 2.1.

While Figs. 6–18 show quantitative information, Figs. 19–22 give an overall qualitative view of the responses that can be expected from each of the procedures. These figures show the following responses:

1. Results for mixed GFEM C^k/C^0 $p = (3;2)$ and GFEM C^k/C^0 $p = (4;3)$, and continuous GFEM, with $p = 3$ and 4;
2. For each of the above formulations, the following results are shown:
   (a) Normalized in-plane stress $\sigma_{xo} = \sigma_x H^2/(qa^2)$ at the outer surface $z = H/2$;
   (b) Normalized transverse shear stresses $\tau_{xzo} = \tau_{xz} H/qa$ at the reference surface $z = 0$ obtained by integration of equilibrium equations; and
   (c) Integrated normalized (as above) and scaled stresses.

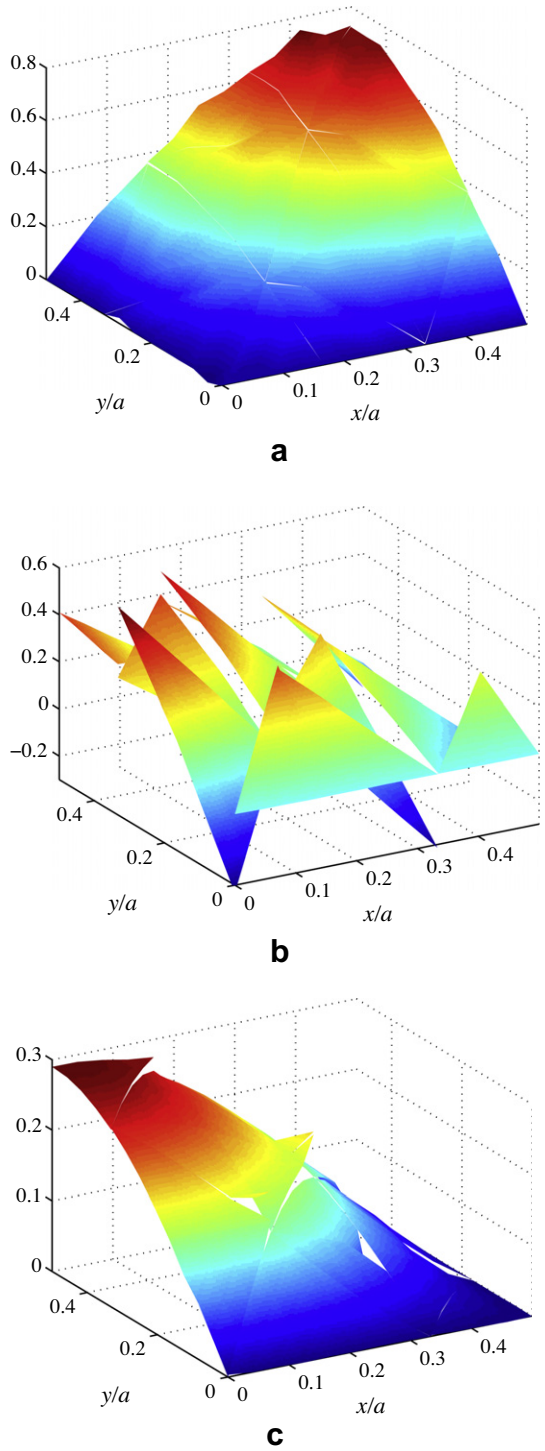

Fig. 19. Results for C^k/C^0 $p = (3;2)$ formulation. (a) Normalized in-plane stress $\sigma_{xo} = \sigma_x H^2/(qa^2)$ at the outer surface $z = t/2$; (b) and (c) Normalized transverse shear stresses $\tau_{xzo} = \tau_{xz} H/qa$ at the mean surface $z = 0$ obtained by integration of equilibrium equations and integrated and scaled, respectively. Triangle integration rule with NIP = 11.2. $M = 3$. Edge function: exponential. $a/H = 4$.

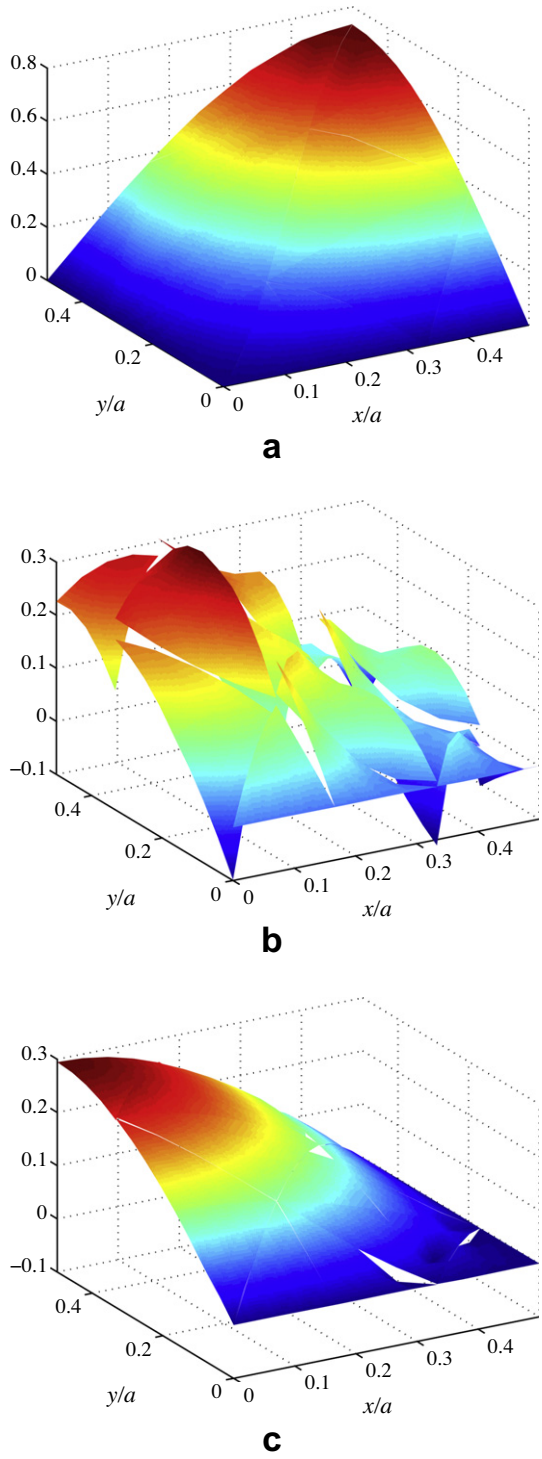

Fig. 20. Results for C^k/C^0 $p = (4;3)$ formulation. (a) Normalized in-plane stress $\sigma_{xo} = \sigma_x H^2/(q^2)$ at the outer surface $z = t/2$; (b) and (c) Normalized transverse shear stresses $\tau_{xzo} = \tau_{xz} H/qa$ at the mean surface $z = 0$ obtained by integration of equilibrium equations and integrated and scaled, respectively. Triangle integration rule with NIP = 11.2. $M = 3$. Edge function: exponential. $a/H = 4$.

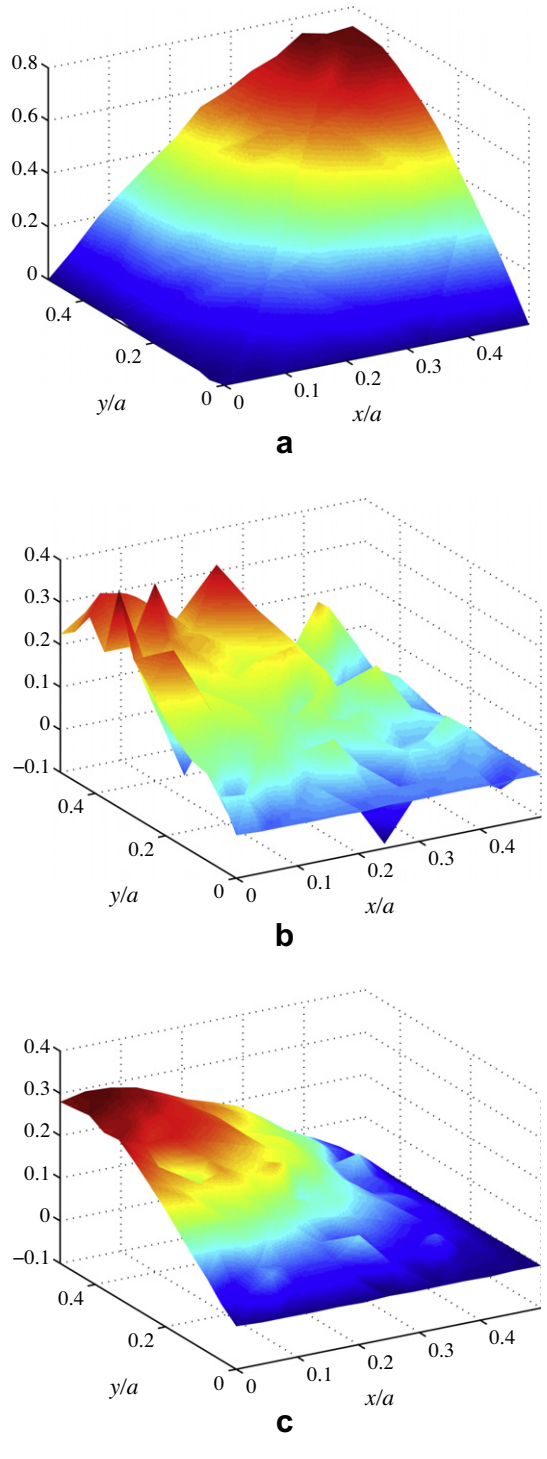

Fig. 21. Results for C^K $p = 3$ formulation. (a) Normalized in-plane stress $\sigma_{xo} = \sigma_x H^2/(qa^2)$ at the outer surface $z = t/2$; (b) and (c) Normalized transverse shear stresses $\tau_{xzo} = \tau_{xz} H/qa$ at the mean surface $z = 0$ obtained by integration of equilibrium equations and integrated and scaled, respectively. Triangle integration rule with NIP = 11.2. $M = 3$. Edge function: exponential. $a/H = 4$.

In all four figures, the results for continuous or mixed GFEM, for both enrichment degrees, show qualitatively reasonable estimates for the in-plane stresses, as expected. The approximations for the simply integrated transverse shear stresses obtained from the discontinuous GFEM C^0 formulations (Figs. 19b and 20b) show, on average, some resemblance of the corresponding exact smooth distribution, but are still crude, particularly the approximation using the $b = 3$ basis. However, even in these discontinuous formulations, the response estimated with the scaling procedure shows a good behavior, even for $b = 3$ (Fig. 19c) with mild interelement discontinuities.

The approximations for the simply integrated transverse shear stresses from the continuous formulations (Figs. 21b and 22b)

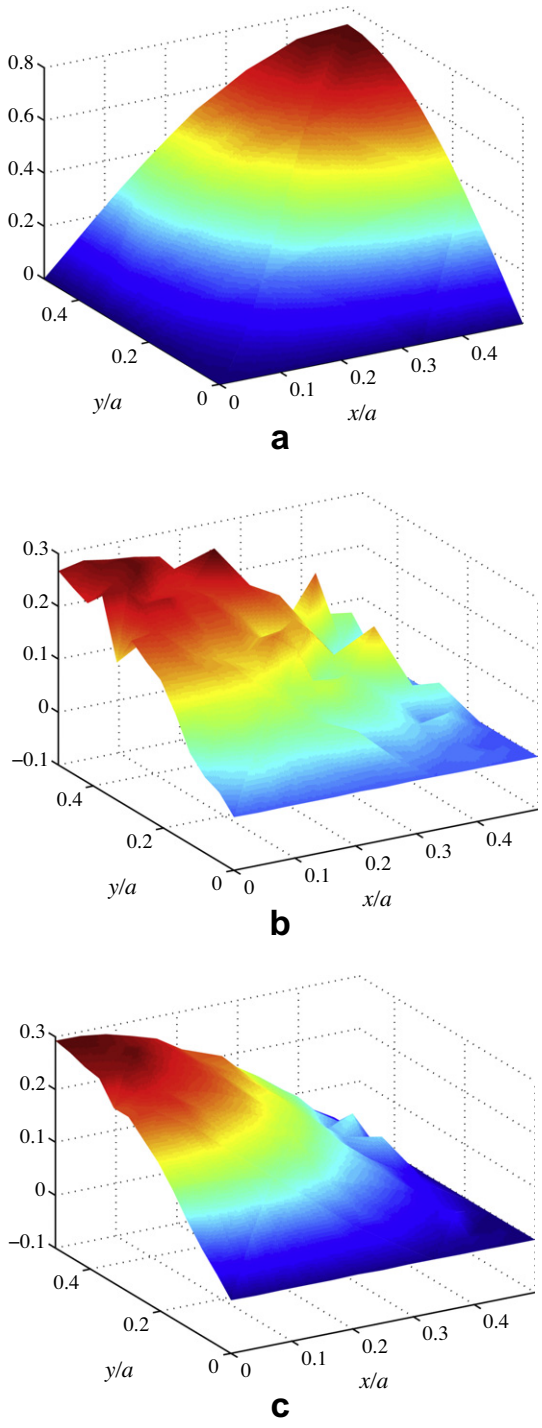

Fig. 22. Results for C^k $p = 4$ formulation. (a) Normalized in-plane stress $\sigma_{xo} = \sigma_x H^2/(qa^2)$ at the outer surface $z = t/2$; (b) and (c) Normalized transverse shear stresses $\tau_{xzo} = \tau_{xz} H/qa$ at the mean surface $z = 0$ obtained by integration of equilibrium equations and integrated and scaled, respectively. Triangle integration rule with NIP = 11.2. $M = 3$. Edge function: exponential. $a/H = 4$.

are continuous, but seem to require a more accurate analysis with a basis of higher degree. However, the response estimated with the scaling procedure shows a good and almost smooth behavior, even for $b = 3$ (Fig. 21c).

Remark 3. *Mesh distortion and locking effects.* This paper is the third in a sequence, where the continuous basis was tested in relation to a C^1 problem (anisotropic laminated Kirchhoff's model [28]) and then to a C^0 problem (anisotropic laminated Mindlin's model [27]). Since the present formulation, based on Reddy's assumptions, is a mixed one, in which the C^0 and C^1 displacement fields are modeled, only some aspects were considered to deserve numerical evaluation. Other aspects, such as integrability, sensitivity to mesh distortion and response under thickness variation, were investigated in detail in the previous papers. In particular, the GFEM C^k shows extreme robustness with regard to mesh distortion, being able to withstand elements much more distorted than the elements produced by any commercial codes. Also, several aspects contribute to the reduced sensitivity of the method with increasing plate thickness. Both behaviors are related to the characteristics of the method, being enriched with functions defined in global coordinates, and the PoU is defined without the use of intrinsic coordinates. Thus, the ability of the basis to model the polynomial degree associated with its enrichment is maintained, with little loss under extreme mesh distortion. Also, as known for the framework of FEM, a higher degree basis is naturally more resistant to any type of locking. With GFEM C^k it is possible to see that even enrichment degrees of $p = 3$ and 4 are sufficient to reduce the sensitivity to thickness of the response.

5. Concluding remarks

An extension of the Generalized Finite Element Method, GFEM, which generates approximation functions with an arbitrary C^k continuity over meshes of triangular elements was used to model the bending problem of arbitrary anisotropic laminated composite plates, under the kinematic hypothesis of the Third-order Plate Theory proposed by Reddy. This model only involves the same five generalized displacement components $(u^o, v^o, w^o, \psi_x, \psi_y)$ as in the first order models (like Mindlin's) and, at the same time, its third degree variation of in-plane displacements across the thickness enables it to provide improved displacements and layer-wise stress estimates in relation to the first-order models. However, it shows two main limitations: (a) its FEM implementation is somewhat hindered by the need to use a $C^1(\Omega)$ continuous basis for the transverse displacement w^o and (b) it is an equivalent single-layer theory, and thus its approximations for the transverse shear stresses are discontinuous at the interlaminar interfaces, and are non-zero at the laminate surfaces, which is in contrast to the physical requirements.

It was observed that limitation (a) was perfectly met by the characteristics of the C^k GFEM and the second limitation was almost completely overcome. The formulation is based on a Shepard Partition of Unity (POU) with at least C^k continuity, subordinated to clouds defined as patches of elements, and enriched with the same scheme as the *hp*-Cloud Method.

The resultant basis functions naturally exhibit inter-element continuity and can be easily enriched to generate arbitrary *p*-enriched basis. As a consequence, all of the estimated strain and stress fields are naturally interelement continuous, without the need for any heuristic averaging or smoothing operation. The method was implemented with three-node triangular elements, although its fundamental characteristics enable it to be also applied to meshes of arbitrarily shaped quadrangular elements. The computational programming of the continuous functions is encapsulated such that the overall structure of the program is the same as that of the standard displacement FEM, and even more similar to the structure of the standard GFEM formulation.

Two variations in the procedure were tested: (a) in the first, all generalized displacement functions were modeled with a C^k continuous basis and (b) in the second, a mixed C^k/C^0 formulation was tested, where the C^k continuous functions were used only for that variable which required such continuity, the transverse displacement, in order to reduce the computational cost. The

remaining generalized displacements, in-plane displacements and rotations were modeled by the C^0 continuous conventional GFEM formulation. The mixed configuration lacks continuity but showed lower computational cost than that of the continuous form.

The performance of both formulations was illustrated through comparisons with analytic solutions, with special emphasis on the computation of the transverse stress field and shear forces for thick laminates.

The tests showed excellent approximations for the layer-wise stresses. In particular, the possibility of generating basis with a high degree, combined with continuity, enables approximations of the transverse shear stresses to be obtained from integration of the local equilibrium equations which show the correct qualitative response, with zero values at one of the laminate surfaces and inter-element continuity. Additionally, the shear forces obtained were well behaved.

These two characteristics enable a second level of post-processing, generating transverse shear stresses from a scaling procedure applied to the integrated shear stresses. The shear forces obtained from integration of the integrated transverse shear stresses were oscillatory or even discontinuous along the edges depending on whether the complete C^k or mixed C^k/C^0 formulation was used. Nevertheless, the scaled distribution of shear stresses matched the respective analytic results very well, both qualitatively and quantitatively, across the thickness and along the laminate surface. This feature becomes more notable along the edges of the laminate.

Overall, the GFEM continuous formulation tested appears to produce reliable responses in terms of the displacements and in-plane and transverse shear stresses, and preserves the standard FEM program structure, presenting a formal structure that permits easy *p*-enrichment and produces reliable transverse stress resultants even with low order basis (third and fourth). As tested elsewhere in the context of C^0 problems [27], the formulation can work exceptionally well with highly distorted meshes, and thus the analysis can be carried out with the better-behaved meshes generated from standard commercial mesh generators. The GFEM C^k/C^0 procedure shows robustness and deserves investigation with regard to its application in approximating solutions for other higher-order differential operators where only some variables require higher-order derivatives.

Acknowledgments

The authors gratefully acknowledges the Brazilian government agency CNPq (National Council for Scientific and Technological Development) for its support through the Research Projects N.309.640/2006-7, N.140.713/2008-5, N.303.315/2009-1 and N.303.575/2010-7.

References

[1] Reddy JN. On laminated composite plates with integrated sensors and actuators. Eng Struct 1999;21:568–93.
[2] Garção JES, Soares CMM, Soares CAM, Reddy JN. Analysis of laminated adaptive plate structures using layerwise finite element models. Comput Struct 2004;82:1939–59.
[3] Liew KM, He XQ, Tan MJ, Lim HK. Dynamic analysis of laminated composite plates with piezoelectric sensor/actuator patches using the FSDT mesh-free method. Int J Mech Sci 2004;46:411–31.
[4] Liew KM, He XQ, Tan MJ, Lim HK. Dynamic analysis of laminated composite plates with piezoelectric sensor/actuator patches using the FSDT mesh-free method. Int J Mech Sci 2004;46:411–31.
[5] Mindllin RD. Influence of rotatory inertia and shear on flexural motions of isotropic, elastic plates. J Appl Mech 1951;18:31–8.
[6] Reddy JN. A simple higher-order theory for laminated plates. J Appl Mech 1984;51:745–52.
[7] Lee KH, Senthilnathan NR, Lim SP, Chow ST. An improved zig–zag model for the bending laminated composite plates. Compos Struct 1990;15:137–48.
[8] Demasi L. Refined multilayered plate elements based on Murakami zig–zag functions. Compos Struct 2005;70:308–16.
[9] Zhen W, Wanji C. An efficient higher-order theory and finite element for laminated plates subjected to thermal loading. Compos Struct 2006;73:99–109.
[10] Simkins Jr DC, Li S, Lu H, Liu WK. Reproducing kernel element method. Part IV: Globally compatible C^n ($n \geqslant 1$) triangular hierarchy. Comput Methods Appl Mech Eng 2004;193:1013–34.
[11] Beirão da Veiga L, Niiranen J, Stenberg R. A family of C^0 finite elements for Kirchhoff plates I: error analysis. SIAM J Numer Anal 2007;45:2047–71.
[12] Djeukou A, von Estorff O. Assessment of different RPIM parameters for statics analyses of shear deformable laminated composite plates. Comput Mech 2009;44:423–31.
[13] Tang Z, Shen S, Atluri SN. Analysis of materials with strain-gradient effects: a meshless local Petrov–Galerkin (MLPG) approach, with nodal displacements only. Comput Model Eng Sci 2003;4:177–96.
[14] Long S, Atluri SN. A meshless local Petrov–Galerkin method for solving the plate bending problem of a thin plate. Comput Model Eng Sci 2002;3:53–63.
[15] Shiah YC, Hwang W-S, Shiah G-C. BEM stress analysis for thin multilayered composites subjected to inertial loads. J Compos Mater 2009;43:349–66.
[16] Garcia OA, Fancello EA, de Barcellos CS, Duarte CA. Hp-clouds in Mindlin's plate model. Int J Numer Methods Eng 2000;47:1381–400.
[17] Duarte CA, Kim D-J, Quaresma DM. Arbitrarily smooth generalized finite element approximations. Comput Methods Appl Mech Eng 2006;196:33–56.
[18] Edwards HC. C^∞ finite element basis functions. Technical report, TICAM report 96-45, The University of Texas at Austin; 1996.
[19] Shapiro V. Theory of *R*-functions and applications: a primer. Technical report 91-1219, Ithaca (NY): Computer Science Department, Cornell University; 1991.
[20] Babuška I, Melenk JM. The partition of unity finite element method: basic theory and applications. Comput Methods Appl Mech Eng 1996;139:289–314.
[21] Melenk JM. On generalized finite element methods. Ph.D. Thesis. College Park: University of Maryland; 1995
[22] Oden JT, Duarte CA, Zienkiewicz OC. A new cloud-based hp finite element method. Comput Methods Appl Mech Eng 1998;153:117–26.
[23] Belytschko T, Black T. Elastic crack growth in finite elements with minimal remeshing. Int J Numer Methods Eng 1999;45:601–20.
[24] Moës N, Dolbow J, Belytschko T. A finite element method for crack growth without remeshing. Int J Numer Methods Eng 1999;46:131–50.
[25] Rvachev VL, Sheiko TI. *R*-functions in boundary value problems in mechanics. Appl Mech Rev 1995;48:151–88.
[26] Torres DAF, Mendonça PTR, de Barcellos CS. Evaluation and verification of an HSDT-Layerwise generalized finite element formulation for adaptive piezoelectric laminated plates. Comput Methods Appl Mech Eng 2011;200:675–91.
[27] Mendonça PTR, de Barcellos CS, Torres DAF. Analysis of anisotropic Mindlin plate model by continuous and non-continuous GFEM. Finite Elements Anal Des 2011;47:698–717.
[28] de Barcellos CS, Mendonça PTR, Duarte CA. A C^k continuous generalized finite element formulations applied to laminated Kirchhoff plate model. Comput Mech 2009;44:337–93.
[29] Shepard D. A two-dimensional interpolation function for irregularly-spaced data. In: Proceedings of the 23rd ACM national conference; 1968. p. 517–24.
[30] Oden JT, Reddy JN. An introduction to the mathematical theory of finite elements. New York: Wiley; 1976.
[31] Duarte CA, Babuška I, Oden JT. Generalized finite element method for three-dimensional structural mechanics problems. Comput Struct 2000;77:215–32.
[32] Wandzura S, Xiao H. Symmetric quadrature rules on a triangle. Comput Math Appl 2003;45:1829–40.
[33] Ramesh SS, Wang CM, Reddy JN, Ang KK. Computation of stress resultants in plate bending problems using higher-order triangular elements. Eng Struct 2008;30:2687–706.